University of Oxford

Department of Engineering Science

Wall Slip in Pasty Flows

by

Alasdair Michael Walker

St. Catherine's College, Oxford

A fourth year project report submitted for the Master of Engineering Science at the University of Oxford

2007

FINAL HONOUR SCHOOL OF
ENG / ECS / EEM / EMS (delete as appropriate)

DECLARATION OF AUTHORSHIP

You should complete this certificate. It should be bound into your fourth year project report, immediately after the title page. Three copies of the report should be submitted to the Chairman of Examiners for your Honour School, c/o Clerk of the Schools, Examination Schools, High Street, Oxford.

Name (in capitals):

College (in capitals): **Supervisor:**

Title of project (in capitals):

Word count: _____

Please tick to confirm the following:

I am aware of the University's disciplinary regulations concerning conduct in examinations and, in particular, of the regulations on plagiarism. ☐

The project report I am submitting is entirely my own work except where otherwise indicated. ☐

It has not been submitted, either wholly or substantially, for another Honour School or degree of this University, or for a degree at any other institution. ☐

I have clearly signalled the presence of quoted or paraphrased material and referenced all sources. ☐

I have acknowledged appropriately any assistance I have received in addition to that provided by my supervisor. ☐

I have not sought assistance from any professional agency. ☐

The project report does not exceed 10,000 words plus 40 pages of diagrams, photographs etc. ☐

I agree to retain an electronic version of the work and to make it available on request from the Chair of Examiners should this be required in order to confirm my word count or to check for plagiarism.

Candidate's signature: Date: ……..

……..

Acknowledgements

Without the invaluable assistance of a number of individuals, the completion of this project would have been unachievable and I would like to take this opportunity to thank them individually.

I thank my supervisor, Dr Peter Martin, for his guidance and assistance throughout the project. I particularly appreciate the manner in which he educated me and the positive encouragement he provided by relating relevant previous experiences.

I thank Dr Ian Wilson, of Cambridge University, for the donation of a redundant testing rig and Adrian Walker, from the EPSRC, for the delivery and demonstration of a high speed imaging camera.

I would also like to highlight the professional, helpful and efficient work of John Hastings and the workshop team, the stores team and Martyn Miles, the inorganic chemistry glass blower, without which the experimental equipment simply would not have existed.

Lastly, I thank Dr Igor Dyson for use of the department materials testing machine and the tuition provided.

Abstract

Wall Slip in Pasty Flows

by

Alasdair Michael Walker

This project presents work undertaken to evaluate the validity of methods which predict wall slip velocities in the capillary flow of granular pastes. With many extrusion design parameters and constitutive modelling attempts dependant on wall slip behaviour, the determination of slip velocities is an important area.

There have been many cases where the classic analysis of Mooney has yielded unviable slip velocities and the alternative Jastrzebski interface condition has been used. It is proposed that the Jastzebski method of analysis may have only been a convenient fit to data for a particular range of experiments and that its use in modern wall slip analysis may provide wall slip velocities, which whilst viable, are incorrect.

The development of an experimental procedure for observing slip velocities visually using a colour marking method is described. This procedure has then been applied to a granular paste consisting of potato granules and water and the observed slip velocities compared to those predicted by the Jastrzebski method and a similar method known as the floating power method.

The velocities predicted by the Jastrzebski method were wholly unviable, whilst the floating power method generated viable, but inaccurate slip velocities. The project has successfully been able to show the ineffectiveness of a Jastrzebski based method for one material over a particular range of wall shear stresses.

Contents

Notation

Roman

A_{barrel}	cross sectional area of barrel
D	inner capillary diameter
D_0	inner barrel diameter
K	Herschel-Bulkley constant
L	total capillary length
$L_{capillary}$	length over which visual slip velocities are observed
m	floating power index
n	Benbow-Bridgewater slip velocity index
P	extrusion pressure
Q	volumetric flow rate
Q_{slip}	component of volumetric flow due to slip
r	general radial co-ordinate in cylindrical polars
$t_{extrusion}$	time taken for transition line to cover $L_{capillary}$
V_{beam}	compressive velocity of cross beam and connected piston
V_{shear}	component of velocity due to shear
V_{slip}	component of velocity due to slip
x	general cartesian co-ordinate

Greek

β	Benbow-Bridgewater die land velocity factor
β_f	floating power slip velocity coefficient
β_j	Jastrzebski slip velocity coefficient
$\dot{\gamma}$	shear rate
$\dot{\gamma}_A$	apparent shear rate
Φ	inner capillary diameter
λ	Herschel-Bulkley power rate index
μ	viscosity
σ_{xx}	longitudinal stress
τ	shear stress
τ_0	yield shear stress
τ_w	shear stress acting on material at wall boundary
τ_y	yield shear stress

Figures

Tables

1 Introduction

This project report details the results of a research project attempting to clarify an analytical issue surrounding wall slip in the extrusion of pastes. It is an academic problem that has received relatively little attention from industry, despite being relevant to a wide range of industrial applications. It is therefore hoped that this work and further resulting research will provide some closure on what is currently a subjective area.

A review of the relevant literature is presented in this Section, including a suggested approach to solving the problem and the principal aims of the project. Section 2 details the development and design of the equipment used and is followed in Section 3, by details of the paste materials used and their constituents. The experimental procedures are described in Section 4, with the results of the project and an evaluation presented in Section 5, before reaching the conclusions and recommendations for future work in Section 6.

1.1 Introduction to pastes

A 'paste' or 'concentrated suspension' is considered to be a two phase material in which solid particles are bound together by a continuous viscous liquid binder phase. Naturally, there can exist a wide range of paste consistencies, each dependant on the ratio of solid and liquid phase present. For the purpose of this project, the term 'paste' will now refer to solid/liquid mixtures that exhibit properties similar to those described by Coussot & Ancey (1999) as 'granular pastes'. These are concentrated suspensions in

which the solids volume fraction is high enough to result in strong interactions between particles. Figure 1.1 depicts a conceptual classification of the rheological regimes that dominate when shearing suspensions of varying solid volume fraction and varying shear rate. The granular pastes described represent the marked region of interest.

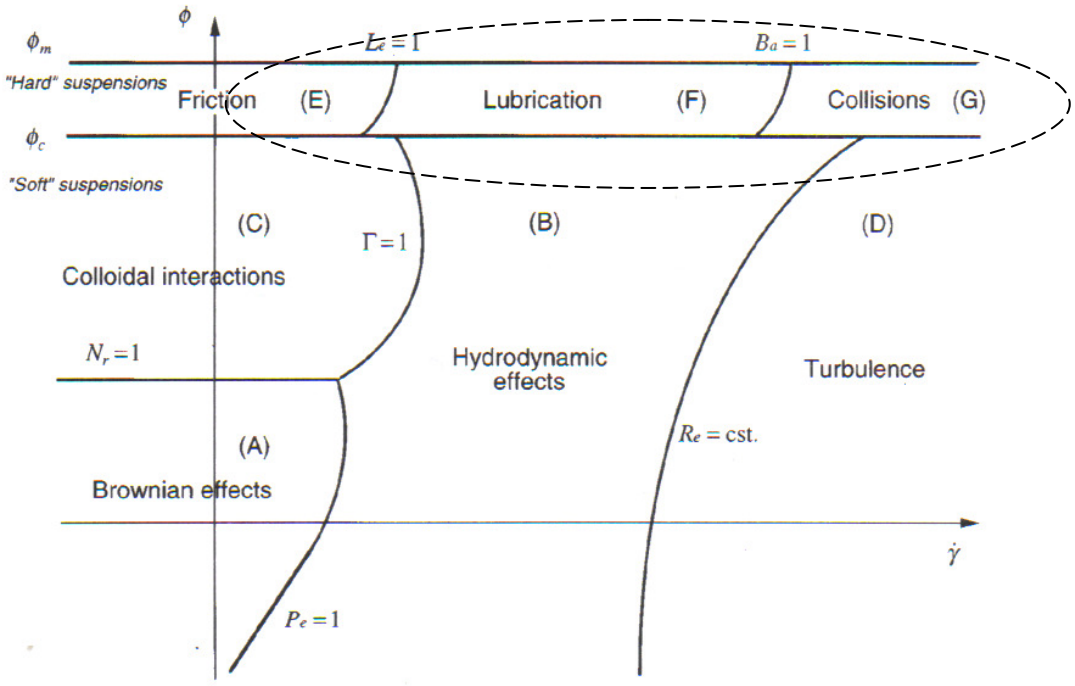

Figure 1.1 Conceptual classification of the rheophysical regimes of a suspension as a function of shear rate and solid fraction on a logarithmic scale. The other characteristics of the suspension are fixed and the limiting curves do not correspond to strict transitions. (Coussot & Ancey, 1999)

The high solid fraction and particle interaction of the pastes described above has the effect of increasing the apparent viscosity of the mixture beyond that of the interstitial medium. Consequently, they can demonstrate viscoplastic behaviour - possessing a yield stress whilst also being readily deformable. Martin et al. (2004) suitably define the relevant pastes as those that possess a yield stress sufficient to prevent deformation of the material under gravity, but may be easily formed into a desired shape and retain their shape until further processing.

The paste properties described provide obvious benefits for production engineering and it is not hard to find applications of paste deformation and extrusion in the production of such items as foodstuffs, ceramics, pharmaceuticals, gels, toiletries and cosmetics. With ample engineering exploitation of paste flows, it is justifiable that rheological study of such flows should seek to improve understanding of related physical phenomena and support attempts at constitutive modelling for process optimisation.

1.2 Flow properties of pastes

The basic flow behaviour of a paste is often found to be a superposition of the individual behaviours associated with the two phases present. Figure 1.2 shows some of these individual behaviours when considering the shear stress developed in the material, τ, as a function of shear rate, $\dot{\gamma}$. For a 'perfect plastic' solid phase, the shear stress during shearing is constant at the yield stress, τ_y. By comparison, a Newtonian fluid displays a linear relationship between shear stress and shear rate, given by:

$$\tau = \mu\dot{\gamma} \tag{1}$$

where μ is the viscosity of the fluid.

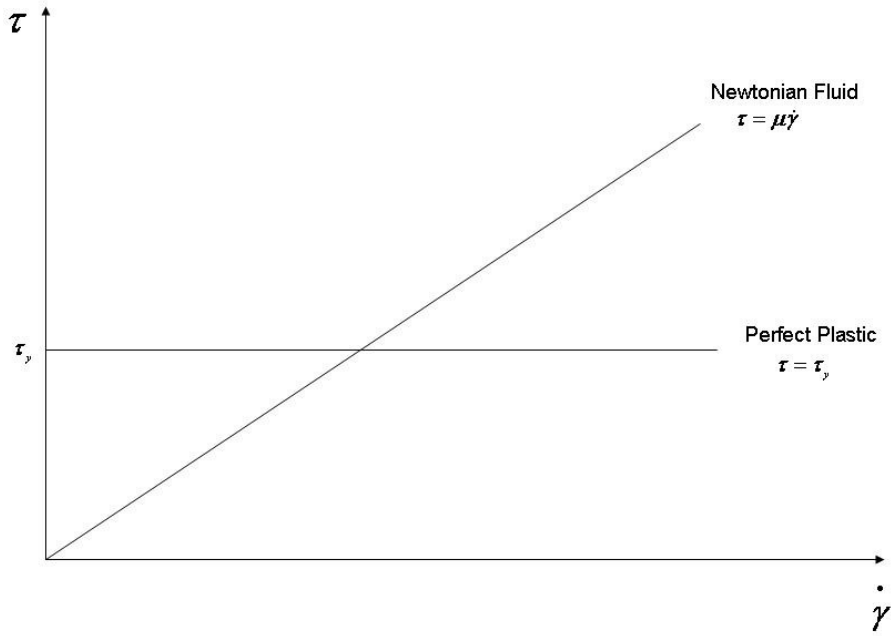

Figure 1.2 A plot of shear stress against shear rate for a perfect plastic solid and a Newtonian fluid

A material that demonstrates a superposition of these two ideals - an apparent yield stress with a linear shear rate dependence, is known as a 'Bingham plastic'. However, when considering a two phase paste, dilation effects can lead to varying voidage between slip planes. 'Shear thickening' relates to increased shear stresses with shear rate whilst the reverse effect is known as 'shear thinning'. For example, many cosmetic products such as creams or gels exploit the effect of shear thinning to remain conveniently viscous for packaging and storage whilst thinning upon application to the skin at a suitable shear rate. This effect can be accounted for by a power law rate dependence and a material which combines all of the above properties can be described by the convenient Herschel-Bulkley model (Herschel & Bulkley, 1926):

$$\tau = \tau_y + K\dot{\gamma}^{\lambda} \tag{2}$$

Figure 1.3 depicts a typical shear thinning Herschel-Bulkley material.

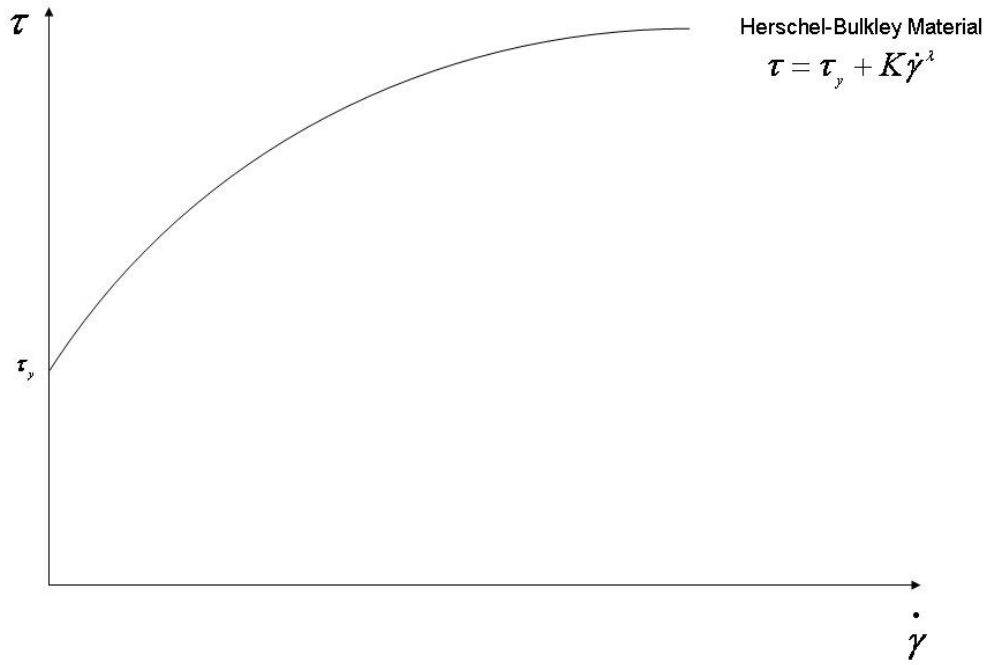

Figure 1.3 Flow behaviour of a typical Herschel-Bulkley material

Whilst convenient, the Herschel-Bulkley model is not comprehensive, since it is an attempt to model two phase pastes with a single constitutive equation. This is often adequate for the bulk fluid, which can be approximated as a single phase, but can be compromised in regions exhibiting two phase behaviour such as wall slip and phase migration. These difficulties are also highlighted by Wilson & Rough (2006), who cite and discuss wall slip, surface fracture and liquid phase migration, as examples of phenomena which compromise extrudate properties, as well as complicating rheological measurement and constitutive modelling. Wall slip is introduced below and phase migration is discussed in Section 5.4 when evaluating methods of slip velocity analysis.

1.3 Wall slip

The phenomenon of wall slip in a capillary is associated with the presence of a wall layer where there is a higher volume fraction of liquid, as depicted in Figure 1.4. This liquid-rich region at the interface has a much lower viscosity than the bulk fluid and therefore facilitates a high shear region when flowing through a capillary.

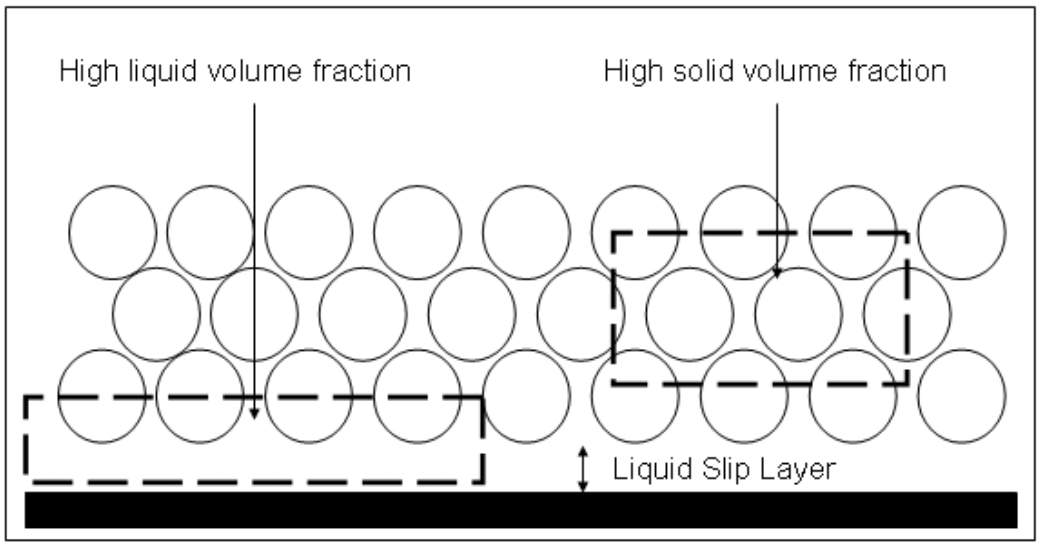

Figure 1.4 Schematic drawing showing solid particle packing in a paste and the presence of a liquid slip layer

Wilson & Rough outline a general problem of pastes in process engineering; there is a lot not yet understood about pastes and, as yet, there is no direct step between processing and product characteristics without a significant degree of experimentation. The noteworthy work of Benbow & Bridgewater (1993) went some way to bridging this gap by proposing framework relationships that allow paste characterisation and physical interpretations such as,

$$\tau_w = \tau_0 + \beta V_{slip}^n \tag{3}$$

There are benefits to be derived from the exploitation of wall slip, including reduced extrusion pressures and with paste characterising parameters dependant upon slip velocity, the quantification of slip velocities is therefore an important area.

1.4 Mooney theory

The first attempt at determining slip velocities from experimental data using a derived model came from Mooney (1931). His formulae were presented for use with a capillary viscometer and required conditions of no turbulence, homogenous material and similar surfaces, so that, as he hypothesised, "the slip shall depend upon shearing stress only".

The resulting Mooney equation (4) (derived in Appendix 1) shows that the total flow rate is comprised of two component terms: a contribution due to wall slip (the first term) and a contribution due to bulk shear (the second term). This behaviour is depicted in Figure 1.5.

$$Q = \frac{\pi D^2}{4} V_{slip} + \frac{\pi D^3}{8\tau_w^3} \int_{\tau_0}^{\tau_w} \left(\frac{\tau - \tau_0}{K} \right)^{\frac{1}{\lambda}} \tau^2 d\tau \tag{4}$$

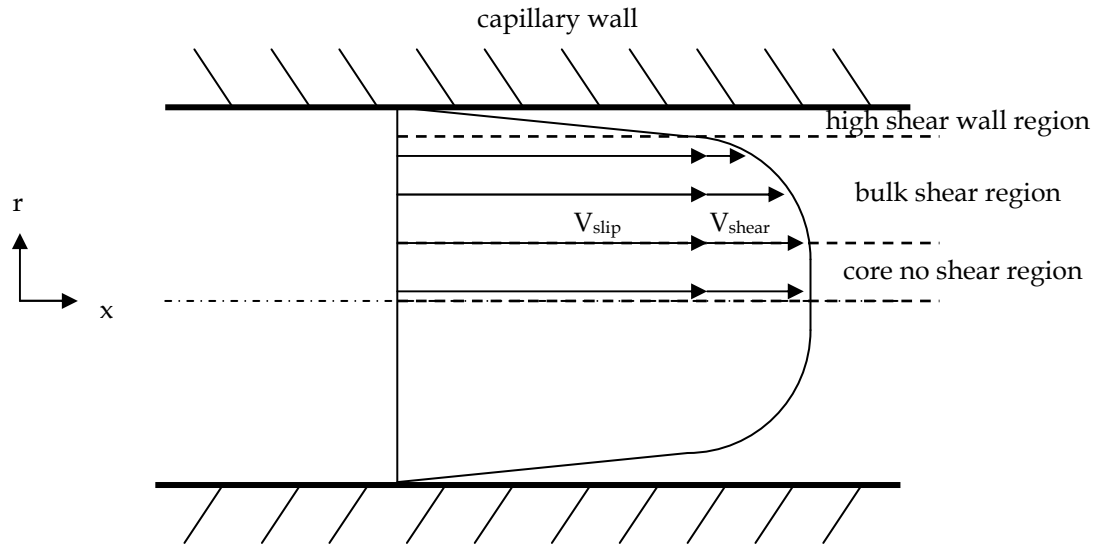

Figure 1.5 Generalised capillary flow pattern

The Mooney equation is often more conveniently expressed as:

$$\frac{32Q}{\pi D^3} = \frac{8}{D}V_{slip} + \frac{4}{\tau_w^3}\int_{\tau_0}^{\tau_w}\left(\frac{\tau-\tau_0}{K}\right)^{\frac{1}{\lambda}}\tau^2 d\tau \qquad (5)$$

The left hand term, $32Q/\pi D^3$ is sometimes called the apparent shear rate, $\dot{\gamma}_A$. Equation (5) indicates that given flow rates for constant wall shear stress in a set of capillaries with a range of diameters, a plot of $\dot{\gamma}_A$ against 8/D will yield a straight line with a gradient equal to V_{slip}.

1.5 Experimental method

The usual setup for capillary flow experiments of this nature involves a reservoir of material connected to a capillary die land, which is reduced in volume at a known rate and pressure by a controllable piston, forcing the material to flow through and out of the capillary (see Figure 1.6)

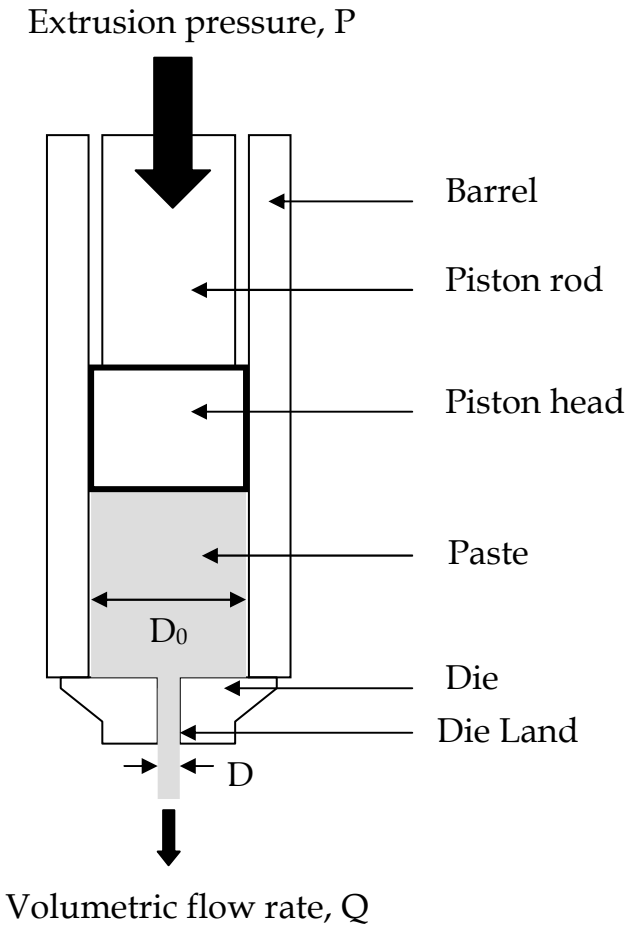

Figure 1.6 Cross-section of a ram extruder with a square entry die

However, the extrusion pressure is made up of both the wall shear stress and the entry effect of compacting the paste from the large volume to a smaller one. Consequently, it is difficult to control the wall shear stress directly when obtaining the necessary data for a Mooney plot at constant wall shear stress. An approach to achieving this is to construct 'Bagley plots'.

Considering equation (15) of Appendix A.1, if it can be assumed that the entry effect is not dependant on the absolute pressure and that the wall shear stress is constant along the length, then the equation can be re-written as:

$$\sigma_{xx} = entry \quad term + 4\frac{L}{D}\tau_w \tag{6}$$

Therefore, if a series of experiments are carried out at constant flow rate and capillary diameter with varying length to diameter ratios, a plot of observed steady state pressure against L/D will yield a straight line with gradient four times the wall shear stress. These experiments can then be repeated over a range of flow rates and capillary diameters to provide wall shear stress vs. apparent shear rate data such as Figure 1.7

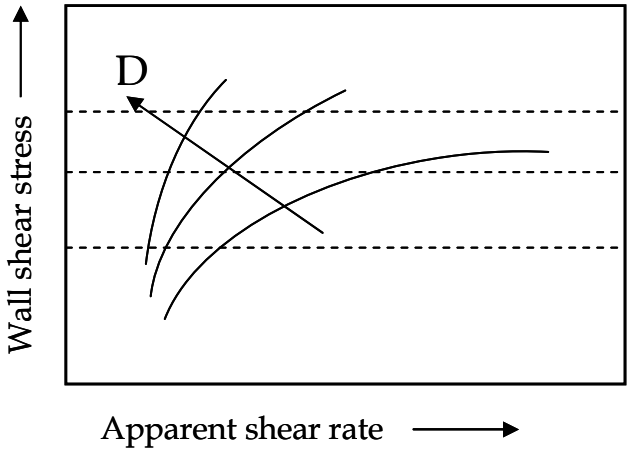

Figure 1.7 Flow curves of capillary wall shear stress against apparent flow rate

From such a plot, apparent shear rates and corresponding capillary diameters can be read off for constant values of wall shear stress. It is then this data which can be used to construct Mooney plots.

1.6 Mooney analysis in the literature

Mooney managed to successfully apply his method to rheological data gathered using a concentrated clay suspension of Kaolin and water. However historically, not everybody has been able to generate viable results from their data using the Mooney method. Some have reported failings due to indications of negative bulk shear e.g. Adams et al. (1995), others reporting that the method suggested the volumetric flow due to slip was greater than the overall volumetric flow e.g. Khan et al. (2001). Most notably however, was the work of Jastrzebski (1967) who reported paste flow data from kaolinite platelets and water that did not give linear Mooney plots when plotted in the standard way against 8/D. However, his results did appear to provide linear characteristics when plotted against $8/D^2$. As such, he proposed, without physical reasoning, that the slip velocity was not only a function of wall shear stress, but also inversely proportional to the capillary diameter:

$$V_{slip} = \frac{f(\tau_w)}{D} \tag{7}$$

Despite the lack of any physical justification, this method of analysis (detailed further in Section 5) has been almost unquestioningly adopted as the suitable method of analysis for calculating slip velocities in paste flows where the classic Mooney analysis has yielded unviable results, even becoming a standard protocol in at least one rheology text (Steffe, 1996).

The basis for this project is a paper by Martin & Wilson (2005), in which a critical assessment of the Jastrzebski method is carried out citing a large sample of literature published on the topic. In summary, more successful Jastrzebski-Mooney analyses were reported than classic Mooney analyses.' It was also shown that in many of the cases where classic Mooney analysis had provided unviable results, a recently developed method of numerical analysis based on Tikhnov regularisation (Yeow et al., 2000, 2003) allowed for viable results to be produced.

It is proposed by Martin & Wilson that the Jastrzebski-Mooney method of analysis is nothing more than a convenient fit to data for a particular range of experiments and with no physical foundation, its use in modern wall slip analysis may provide wall slip velocities which, whilst viable, are incorrect. It is acknowledged that the problem of unviable results from the classic Mooney analysis still needs to be addressed, but that the Jastrzebski method has simply hidden, not solved the problem.

1.7 Project aims

This project seeks to extend the work of Martin & Wilson and provide quantitative evidence to support (or indeed refute) their hypothesis regarding the ineffectiveness of the Jastrzebski-Mooney method (work also called for by Wilson & Rough). It hopes to achieve this by developing an experimental procedure for accurately and independently measuring slip velocities so as to compare them to those calculated by the Jastrzebski-Mooney method. Methods for directly obtaining slip velocities suggested by Wilson & Rough and Martin & Wilson include magnetic resonance imaging, confocal microscopy, infrared spectroscopy and direct observation of the flow using coloured markers. Due to practical constraints and financial limitations, it is the last of these options that is most suitable. The method, as outlined below, has been documented by Graczyk et al (2001).

Figure 1.8 depicts the colour marking method schematically. When preparing the paste, a portion is stained with a small quantity of coloured pigment and replaces the unstained paste in the barrel mid-way through an extrusion to create a clear transition line at the die inlet. The extrusion is then resumed and run at a desired flow rate until the separation line reaches the end of the capillary tube. Since the transition line in a three dimensional capillary represents the slip at the wall, the slip velocity can be calculated very simply from:

$$V_{slip} = \frac{L_{capillary}}{t_{extrusion}} \tag{8}$$

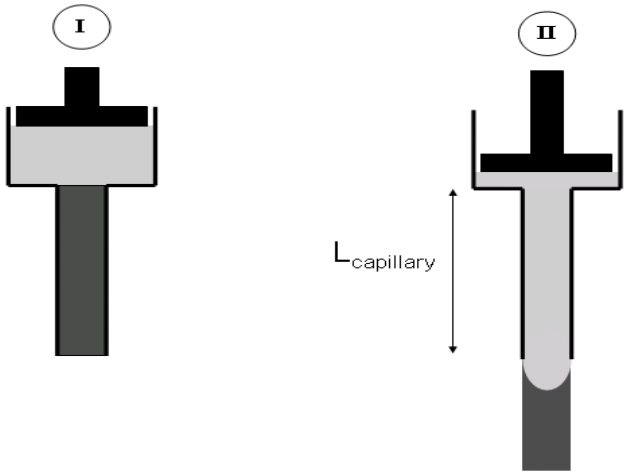

Figure 1.8 Schematic of colour marked cross section in the barrel and die prior to extrusion (I) and after extrusion time, $t_{extrusion}$ (II)

The colour marking method can be run at the same flow rates and diameters used for Mooney plots and direct slip velocities determined for each. These slip velocities can then be directly compared to those predicted by the Mooney and Jastrzebski methods, thereby validating or invalidating their effectiveness at accurately predicting slip velocities in pastes.

2 Equipment Design

The following section outlines the preliminary, design and construction work undertaken to devise a reproducible experimental procedure.

2.1 Developing the test rig

Section 1.5 describes the required experimental setup for the capillary flow analysis of interest, using a controllable piston to extrude paste material from a larger cylindrical reservoir through into a smaller die of known diameter.

In order to accurately control piston movements and simultaneously extract reliable pressure measurements, it was decided that all apparatus would be designed to operate within a materials testing machine. The machine available for use was an Instron 5582. Vertical control of the cross beam (see Figure 2.1) could be exercised using velocity (and hence flow rate) control, displacement control or force control. All of the individual raw data measurements from the load cell could be exported for manual averaging over a chosen range.

Figure 2.1 Instron 5582 materials testing machine

A test rig was now required to accommodate the larger reservoir and dies whilst aligning with a piston to be attached to the cross beam. Fortunately, some redundant equipment was kindly donated by the University of Cambridge, including: a steel frame with base plate and top plate (Figure 2.2); a 25mm diameter steel piston rod with nylon head (Figure 2.3); a brass insert for the top plate (Figure 2.4) and a 25mm diameter cylindrical steel barrel to be used as the larger reservoir (Figure 2.5).

Figure 2.2 Steel test frame with base plate and top plate

Figure 2.3 25mm diameter steel piston rod

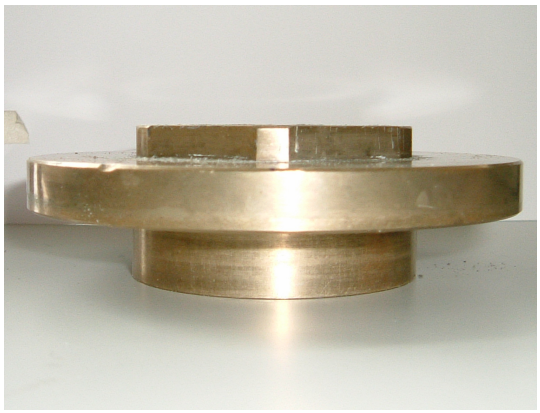

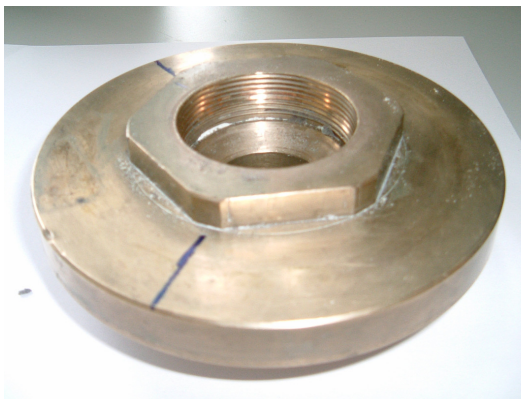

Figure 2.4 Brass insert for top plate

Figure 2.5 25mm diameter cylindrical steel barrel to be used as larger reservoir

The steel frame had previously been designed for use on an alternative testing machine and required modification to be compatible with the base plate mounting of the Instron. So as not to overlap with those existing, new holes were drilled on a 90°orientation, meaning that any experimental viewing would now have to be from the narrow end of the frame, but this was deemed acceptable for the purpose. A high precision central locator was also added to ensure consistent positioning of the frame.

The accompanying cylindrical steel barrel and brass top plate insert were designed to assemble as shown in Figure 2.6, leaving space for an insertable die.

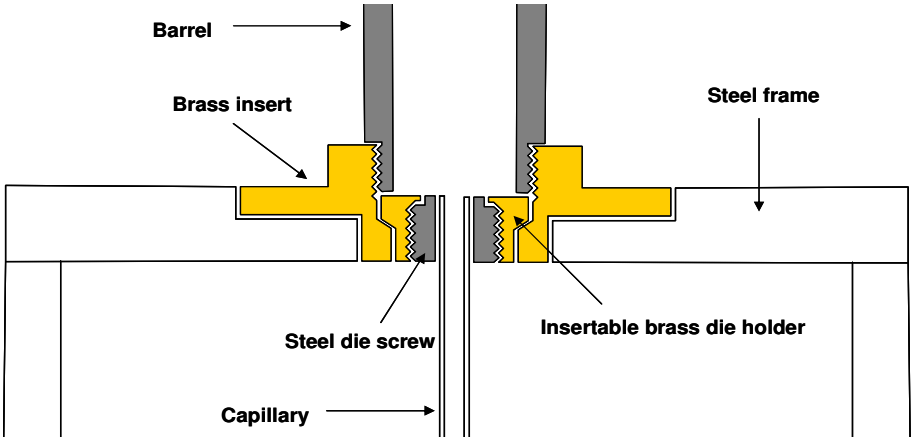

Figure 2.6 Schematic cross section showing the assembly of the frame, barrel and top plate insert

The nylon piston head was received in a deformed condition and so a replica was made. However, to prevent the head deforming under stress again, the replica was machined from brass. Where possible, the design of metal contacts used steel/brass contacts, due to the well-known functional interaction of the two metals.

2.2 Alignment of equipment

Once assembled into the testing machine, the piston was driven down through the barrel at constant velocity over a displacement of 100mm to observe the force profile of the piston only. In order for the piston and barrel to be satisfactory for use, there must be no significant force from the movement of the piston contributing to any force measurements taken for a particular extrusion. After observing the resultant force profile, this was not the case and the piston was clearly not moving smoothly down the barrel.

On closer inspection of the piston rod, a notable bend explained the jumps in force as the bend would have begun to feed into the barrel. After manual attempts to straighten the piston rod using a three point bending machine and a thin shaving off the piston head, the force profile shown in Figure 2.7 was obtained.

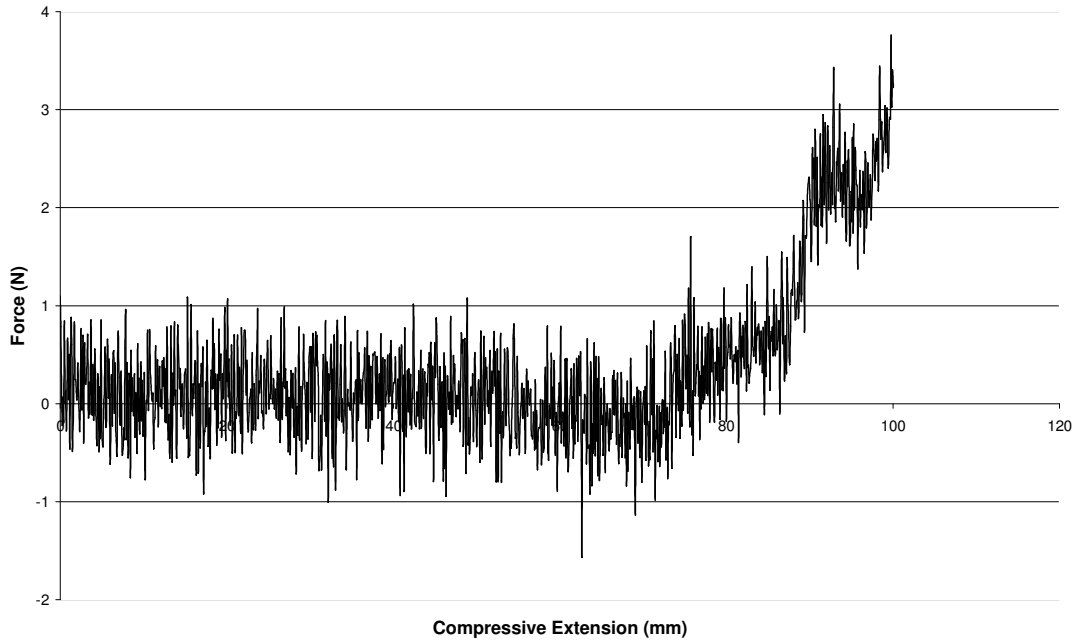

Figure 2.7 The piston-only force profile obtained after piston straightening

Although the piston rod was still not perfectly straight, this profile successfully showed negligible force contributions (when dealing with extrusion forces three orders of magnitude higher) over a displacement range

of 75mm. It was therefore decided that all extrusions would be run over a displacement of 70mm from 5mm below the top of the barrel. The position and orientation of all assembled parts were marked using permanent marker to ensure consistent alignment upon reassembly for each extrusion.

2.3 Designing the dies

It was initially thought that the dies would not have to be transparent to calculate slip velocities visually, since the starting position of the transition line would be known and the extrusion time could be measured from the start of the extrusion to the appearance of the transition line at the bottom of the die. As such, sets of stainless steel tubing ranging in diameter from 2.4mm to 5mm were bonded into machined steel screw heads using Loctite, as shown in Figure 2.8.

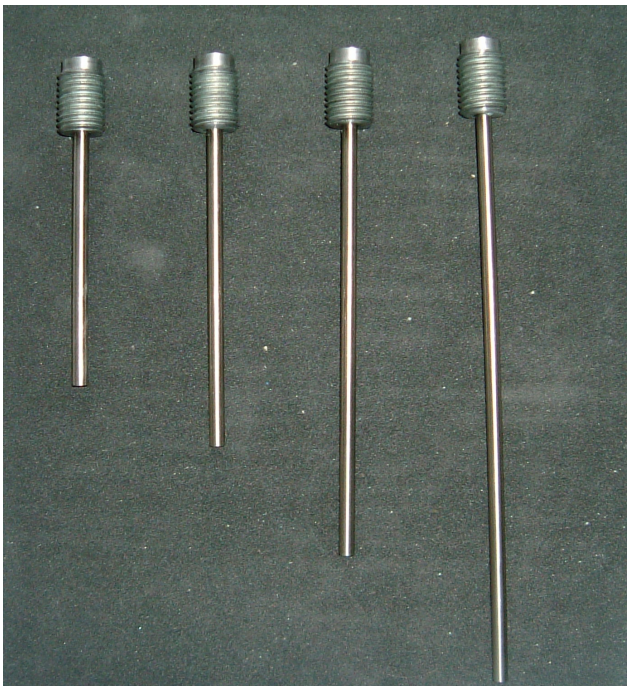

Figure 2.8 Four examples of steel tubing dies with constant diameter and varying L/D ratios

However, when conducting preliminary experiments to evaluate the procedure, difficulties were found in controlling the start position of the piston head so as to instantly start/resume an extrusion without a spatial or compressive delay. Consequently, it would be impossible to specify the time at which the transition line began to move for the visual experiments. As such, it became clear that transparent dies were required so the transition line could be viewed along the capillary, and for clarity of vision, glass was chosen.

A number of Mooney analyses in the past have conducted experiments over three diameters and three L/D ratios producing only three points on a Mooney plot. This can make interpretation of a Mooney plot very difficult when deciding if a trend is linear. As such, a set of 25 glass capillaries were ordered from the glass blower, covering five diameters and L/D ratios to give five points on any subsequent Mooney plot.

However, a clerical error in the ordering process meant a mixed set of capillaries were received that did not match the original specifications. In order to save the time of remaking the capillaries, those received were measured manually using a set of vernier calipers at the measurement points shown in Figure 2.9.

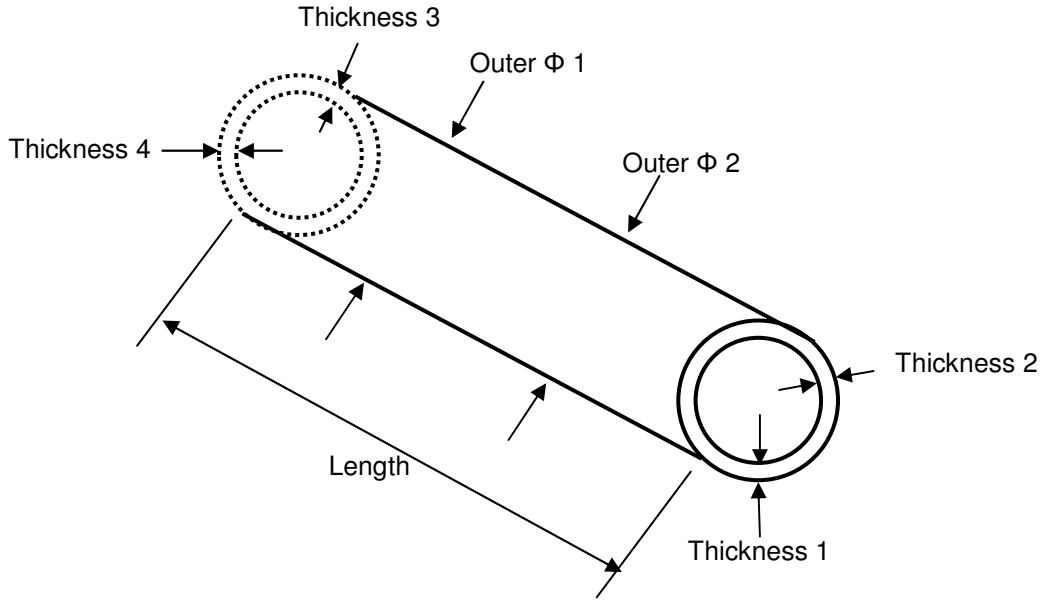

Figure 2.9 Measuring points for the glass capillaries received

All of the measurements were recorded and it was attempted to select a set of capillaries that best matched constant diameters and L/D ratios. The average of wall thicknesses 1,2,3 and 4 was subtracted from the average outer diameter to calculate each inner diameter.

A set of four diameters and L/D ratios were successfully selected for which the deviations from the average were considered acceptable. Table 2.1 shows the measurements of the 16 capillaries chosen. The average inner diameter is shown down the left hand column with the average L/D ratio along the top row. For each capillary, the top number represents the measured L/D ratio and the bottom number represents the measured inner diameter.

L/D / Φ(mm)	**26.21**	**30.4**	**39.4**	**50.75**
2.44	26.1 (2.47)	30.0 (2.39)	40.3 (2.39)	51.1 (2.51)
2.84	26.1 (2.82)	31.3 (2.87)	37.4 (2.90)	49.5 (2.75)
3.93	26.0 (3.87)	30.5 (3.93)	39.8 (3.99)	51.3 (3.93)
4.83	26.7 (4.90)	30.0 (4.85)	40.0 (4.88)	51.2 (4.71)

Table 2.1 Manual measurement of diameters and L/D for selected glass capillaries. For each capillary, the top number represents the measured L/D ratio and the bottom number represents the measured inner diameter.

It was decided to first try bonding the glass capillaries to the screw fittings with silicone sealant, due to its strong contact with glass and resistance to water. Unsure of whether to use steel or brass for the fittings and with no data found relating to the shear strength of silicone sealant bonded to particular metals, a few prototypes were assembled using simple machined pieces of brass/steel and solid glass rods. After 24 hours curing time, the prototypes were tested by hand. The rod bonded to the brass failed

with very little force and the result is shown in Figure 2.10. The uniform shape of the sealant around the glass rod shows that it was the brass which the sealant had failed to adhere to sufficiently. The rods bonded to steel fittings required a much larger force, but still failed by hand.

Figure 2.10 Failed prototype for bonding glass to brass using silicone sealant

Closer inspection of the remaining silicone on the glass rods showed significant amounts of uncured sealant. This may have been due to the relative lack of oxidation available in the enclosed bond area.

Allowing some of the prototypes to cure in an oven at 200°C for three hours had an improved effect on the strength of the bond and it was no longer shearable by hand. However, after bonding some actual capillaries in this fashion and extruding with the stiff test paste first considered (see Section 3), there was considerable unpredictability over which bonds held and which failed. Silicone sealant was not an acceptable adhesive.

The glass capillaries were cleaned after being coated with silicone sealant remover and an alternative adhesive was considered. Since it was thought that a lack of oxidation was responsible for the uncured sealant, an

adhesive which cures by chemical reaction seemed appropriate and a two part epoxy resin (Araldite) was used.

The strength of bond provided by the epoxy resin was considerably higher than that of the silicone sealant and more than suitable for the purpose. To improve the chance of successfully obtaining a data set which could be analysed fully, the paste material was also changed as discussed in Section 3.

For the visual measurement of slip velocities using the colour marking method, the movement of the transition line must be timed over a known distance. As such, thin pieces of tape were placed around the glass capillaries and the distance from the bottom of the tape to the end of the capillary was measured using vernier callipers as $L_{capillary}$. A compromise had to be reached between reducing the margin of error by maximising the distance and time and allowing sufficient opportunity for the paste to resume steady flow. Examples of this compromise are shown in Figure 2.11.

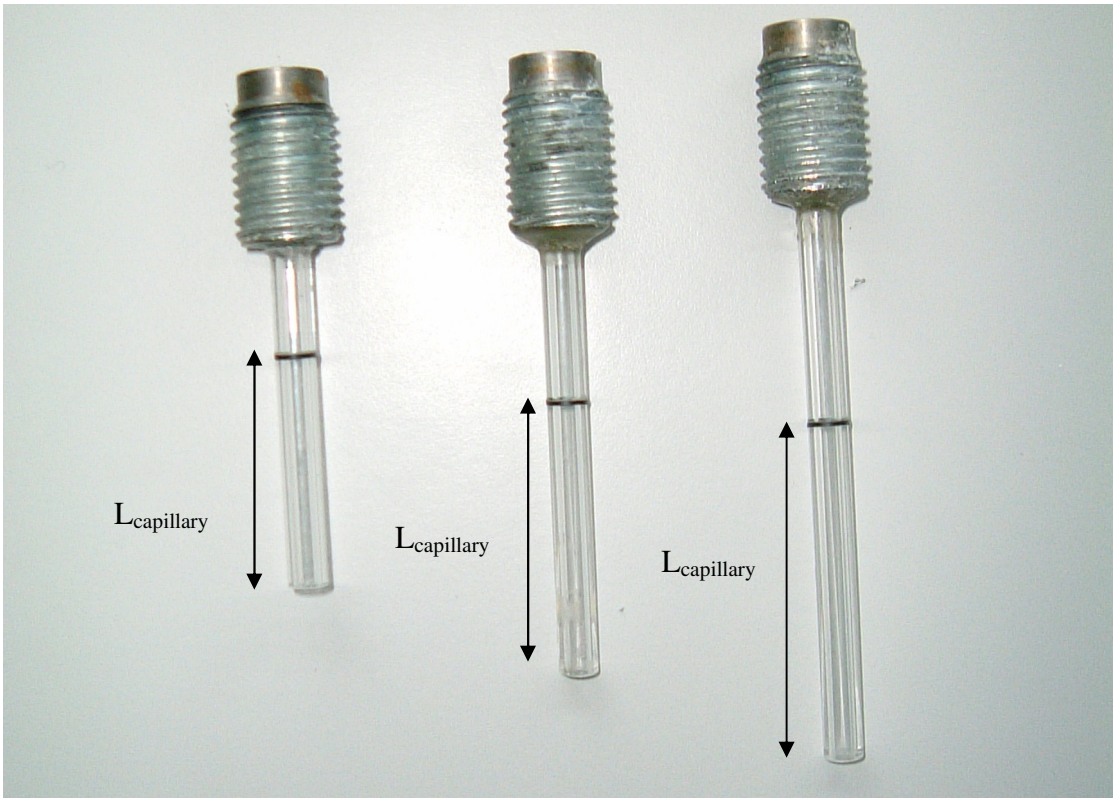

Figure 2.11 Three glass capillaries with marked $L_{capillary}$

2.4 High speed imaging camera

A high speed Kodak EM imaging camera, capable of recording at up to 1000fps was secured for accurately timing the movement of paste transition lines. The camera setup is shown in Figure 2.12 with a white background and side lighting used to reduce glare. The high power of the spot lights used meant they could only be switched on for adjusting the camera picture and immediately before an extrusion due significant heating of the glass dies and paste within them.

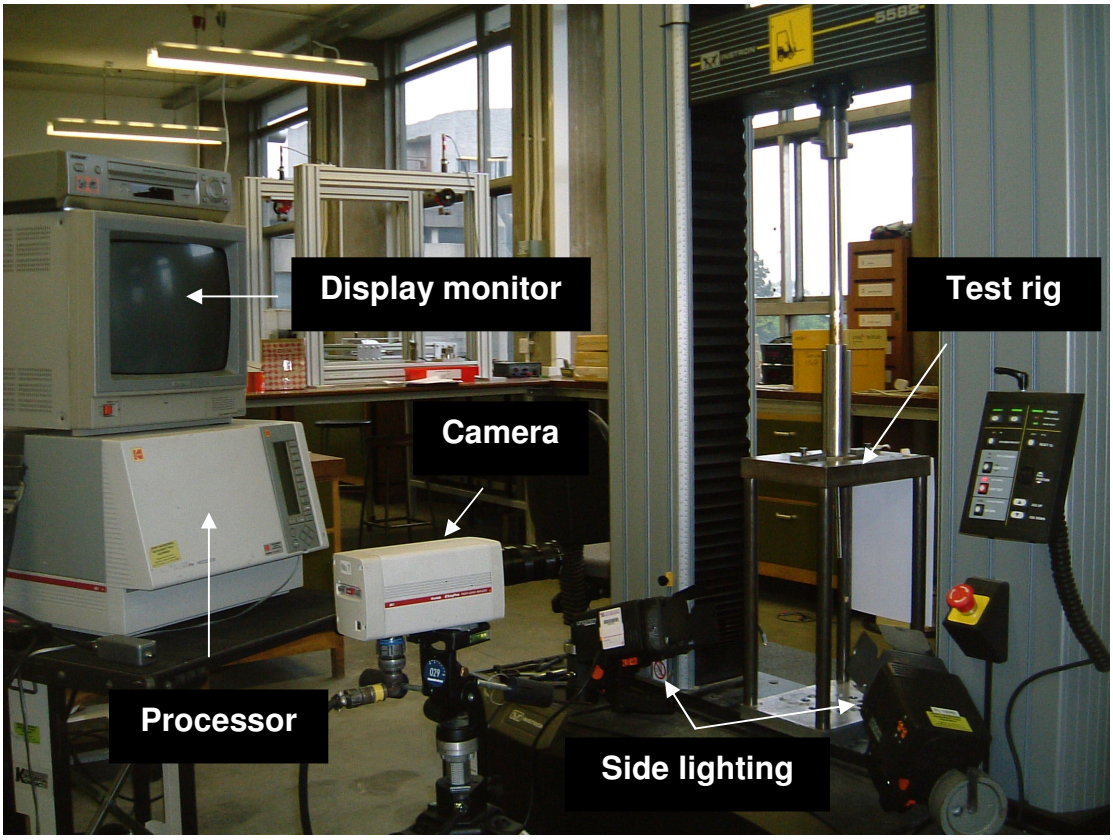

Figure 2.12 Visual camera setup

3 Paste materials and their constituents

In previous work undertaken by Martin (2002), the material of choice had been a paste consisting of Magnesium Silicate (Talc powder), surfactant and water, designed to model an industrial paste used in the production of Water Dispersible Granules (WDGs) for agricultural crop use. In this work, Martin found the paste to yield unviable classic Mooney plots, but was successful in compiling Mooney diagrams based on the Jastrzebski interface layer condition. With a substantial quantity of Talc powder accessible free of charge, it was decided that a similar paste mixture using Talc and water would be a suitable starting material to investigate. The necessary COSHH assessment form is completed in Appendix 2.

Data available from Martin showed the viscosity of the liquid phase in said paste was higher than that of water alone. Suspecting that the lower viscosity of a solely water liquid phase might lead to excessively quick drainage from the paste, it was decided to match the viscosity of the liquid phase to that of Martin's paste using an appropriate concentration of aqueous glycerol solution.

3.1 Talc paste composition

The viscosity of the liquid phase used by Martin was 13.4cP. By using linear interpolation between data charting the varying viscosity of different aqueous glycerol solutions (Segur & Oberstar, 1951), it was found that a solution of 63%wt. glycerol was required to achieve a viscosity of 13.4cp.

By solving simultaneous equations for total volume and glycerol concentration to examine the form of the most viscous paste permissible by Martin & Wilson's (2005) (a solid volume fraction of 0.4), the composition shown in Table 3.1 was developed.

Constituent	Fraction (wt.)
Micro-Talc AT Extra	0.627
Glycerol	0.235
Water	0.138

Table 3.1 Talc paste constituents

Mixed in these proportions, the talc paste resembled a clay or very dense plasticine, remaining solid, but still pliable. Upon mixing samples of this paste, it seemed as though it would be fit for the purpose. However, as previously described in Section 2.3, the extrusion pressures required to pass this paste through the capillaries were too large for the sealant on many capillaries to hold.

3.2 Changing the material

To improve the chances of creating a setup that held in place throughout extrusions, it was decided that an alternative, less viscous material should be used in addition to an alternative adhesive. With time and resources as limiting factors at this point, a new choice of material had to be cheap and readily accessible. After reviewing all of the solid/liquid pastes summarised by Martin & Wilson (2005), two reported cases of potato granules

and water were found: one where Mooney analysis had been conducted successfully (Corfield et al. 1999) and one where it had not (Halliday & Smith 1995, 1997). The Jastrzebski interface condition had not been applied to either case. Despite there being other readily available pastes such as apple sauce (Kokini & Plutchok, 1987) and butter (Shukla & Rizvi, 1995) which had been successfully analysed using the Jastrzebski condition, it was felt that potato granules and water offered the greatest chance of successful extrusions and the greatest degree of control over composition and consistency.

3.3 Potato granules and water composition

The potato granules used to form the paste were sachets of Sainsbury's instant mashed potato mix (86% dehydrated potato) and it was thought reasonable to assume that individual packets of the same product would be consistent. However, packaging masses were ignored and all mass quantities measured independently using an electronic balance.

With little data available about the properties of a specific brand of instant mashed potato, the relative proportions of potato granules and water were determined by trial and error. This was done so as to best fit the specific requirements of the project whilst still satisfying the qualitative description of a highly filled paste taken from Martin et al. (2004) in Section 1.1. The paste product had to satisfy five main requirements:

- The consistency must remain sufficiently viscous to prevent deformation under gravity alone.
- It must also be pliable for experimental handling without crumbling.
- For experimental performance, the paste must remain sufficiently dry so as not to exhibit liquid phase drainage or distortion of the transition line when conducting visual experiments.
- The paste must be sufficiently viscous for the extrusion pressure not to cause the capillary adhesive to fail.

- For experimental consistency, the paste must not change composition significantly over the handling time and must be consistent across separate batches.

Table 3.2 details the constituent quantities for each batch of potato granules and water paste used throughout all subsequent experimentation.

Constituent	Batch Quantity
Sainsbury's instant mashed potato mix	890g
Water	1500ml

Table 3.2 Potato granule and water quantities

3.4 Mixing process

The mixing process, which was identical for each batch of paste, was as below. All mixing took place in a Crypto Peerless industrial planetary mixer on the slowest speed setting available to minimise heating and micro-structural change.

1. All 890g of instant mashed potato granules dispersed evenly into mixing bowl.
2. Mixing attachment initiated.
3. 1500ml water added steadily over a period of 4 minutes to encourage uniform distribution of water within paste.
4. 5 minutes automated mixing.
5. Mixer stopped and paste stirred manually to ensure no granules left in the bottom of the bowl.
6. 9 minutes further automated mixing.
7. Cover with cling film and allow to rest for 30 minutes before use.

3.5 Colour marking

As outlined in Section 1.7, paste batches of two different colours were required for the direct visual measurements of slip velocity and had to provide a distinct transition line when viewed through a black and white camera. The natural colour of the potato paste was a light cream colour which made it likely that any darkening of the potato would provide suitable contrast.

It was initially thought that this darkening could be achieved by mixing small quantities of carbon black powder grated from charcoal rods into the potato paste as it was prepared. However, this proved unsuccessful as large quantities of powder were required to provide sufficient contrast. With such large quantities of carbon mass in the stained paste and none in the unstained paste, the material could no longer be considered homogenous as is one of the principal assumptions of the Mooney model. Hence, an alternative method had to be found.

The next and most successful attempt at colour marking the potato paste was to use small amounts of black liquid food colouring. The colouring was pre-mixed with the water before being added to the potato granules as normal. Of the 1500ml of water used in each batch of paste, only 25ml needed to be replaced by colouring, giving a colouring concentration of 1.6%. This concentration was considered low enough not to significantly affect the flow properties of the paste and could be verified by comparing the two sets of extrusions.

3.6 Water content and consistency

During the course of all final experimentation, the water content of six paste batches was measured immediately after preparation using a pre-heated oven at 220°C. This was done so that the consistency of the preparation method could be evaluated. The initial water concentrations of the six batches samples are shown in Table 3.3.

Batch Number	Water Content (%)
1 – Unstained	66.4
1 – Stained	66.5
2 – Unstained	65.9
2 – Stained	66.6
3 – Unstained	68.5
3 – Stained	68.7
Average	67.1

Table 3.3 Initial water concentrations of six batches of potato sampled

It can be seen that the level of consistency for the first four batches sampled was high, with only a slight variation in the last two. The relative size of the variations were considered small enough to be negligible when analysing the results and for the data to be representative of a potato granule and water paste with 67.1% average water content.

It was found that the length of time left after designing and building equipment, creating a suitable methodology and conducting what are very time intensive experiments, allowed only the one material to be successfully analysed.

4 Experimental method

The following section describes the experimental procedures used in this project. All work was carried out in accordance with the appropriate safety precautions outlined in the risk assessment (see Appendix 3).

All potato was prepared as described in Section 3 and used within eight hours of preparation. The Instron machine was calibrated at the start of every experimental session after removing all fittings from the load cell.

4.1 Non-coloured method

So as to remove joins and pockets of air, the brass die holder was inserted into the test rig ready for paste precompaction, with a bolt screwed in to act as a blank die. The barrel, filled manually with potato, was then screwed into the brass insert, aligning the marks made for consistent assembly. After slowly feeding the piston manually into the top of the barrel, the paste could be compacted at constant velocity until the pressure levelled off and paste began to flow out of the top of the barrel. The piston was then raised and left for one minute before unscrewing the barrel so the potato had chance to fully relax and remain in the barrel once removed.

With the barrel removed, the blank die could be replaced with an experimental die before reassembling and feeding the piston back to a consistent start position. A beaker was placed below the die to collect the extrudate, the force and displacement readings on the Instron zeroed and the extrusion was ready to run.

An extrusion was then run at any one of five predetermined cross beam velocities (see Appendix 4 for conversion from cross beam velocities to flow rates). Once completed, all of the raw data was copied into a spreadsheet file and saved, with the force profile printed and recorded accordingly.

After disassembling the test rig, the barrel was emptied and cleaned before filling with fresh paste. This was found to be necessary for consistent results in the test extrusions. The process was then ready to repeat for a different die. All flow rates were done together in groups but the order in which the diameters and L/D were varied was chosen randomly for each flow rate so as to remove any systematic error.

4.2 Colour marked method

The colour marked extrusions were carried out in the same fashion as above, but with an additional stage to create a transition line between stained and unstained paste. A barrel of unstained paste was compacted and extruded at constant flow rate to fill five capillaries at a time. A filled die was then inserted into the test rig, having wiped the paste flush at the top for a precise transition line and a fresh barrel of stained paste screwed in.

The camera could now be set up to the correct vertical height, aperture setting and zoom (only switching the lighting on when establishing a picture and running the beginning of an extrusion due to the heat generated). Once set ready to record, the experiment was ready to run.

The extrusion was then restarted and viewed on the camera display screen. Once the transition was visible a small distance above the marked start line on the die, the camera was triggered manually to record. As soon as the transition line had passed out of the die, the lighting was switched off and the extrusion left to run over the full range, with the data recorded as for the non-coloured method. The time taken for the transition line to travel over the

known distance $L_{capillary}$ was obtained from playback on the camera display screen.

In the case of the colour marked experiments, the water content of the extrudate was measured (for reasons discussed in Section 5.3). This meant that the mass of the beaker used to collect the extrudate had been recorded prior to an extrusion. The process could then be repeated for another die.

5 Results

This section presents the results obtained from all of the final experiments conducted for the project. It recounts and elaborates on the methods of analysis described in Section 1, illustrating the processes involved and how the data has been interpreted. The data is first compiled and formatted to construct the appropriate Mooney and Jastrzebski plots for predicting slip velocities, before presenting comparable data from direct measurements.

5.1 Extrusion pressures

It is recalled that experiments at constant values of wall shear stress required for use in the Mooney equation (4) are difficult to achieve and that an indirect approach was to be adopted. Equation (6) said that the pressure required for the extrusion of a paste consisted of two components: the energy required to compact and deform the paste and the energy required to overcome friction along the capillary:

$$\sigma_{xx} = entry \quad term + 4\frac{L}{D}\tau_w$$

Subsequently, a series of extrusions were carried out at constant flow rate and capillary diameter with varying length to diameter ratios. The intention was that a plot of steady state pressure against L/D would yield a straight line with gradient four times the wall shear stress. A number of these

'Bagley plots' were constructed for a range of flow rates and capillary diameters to provide a family of curves when plotting wall shear stress against apparent shear rate.

In order for these plots to be constructed, the piston was driven down at constant velocity and the force profiles recorded. It was from these force profiles that a steady state force and hence axial extrusion pressure (division by the face area of the piston), were to be obtained.

A typically well behaved force profile is shown in Figure 5.1(i). It shows a steep initial increase whilst the paste compacts and fills the capillary, before levelling out at a steady state value. It is clear from this where steady state has been reached and the vertical lines mark a range over which the extrusion force could be averaged.

However, as previously described in Section 2.2 the piston rod and barrel were susceptible to a certain degree of bending and whilst it was attempted to reduce this effect as much as possible, it could be clearly seen to affect the behaviour of some profiles. Figures 5.1 (ii)/(iii) show examples of profiles where this occurred, both where the force required to pass through the barrel increased suddenly and gradually. For profiles such as these, the force was averaged over a range nearest the start of the plateau, as it was felt that these were the regions that most closely reflected the true extrusion force before being compromised by additional components. In a few rare instances, such as Figure 5.1(iv), no clear steady state range could be observed and data from these extrusions was ignored.

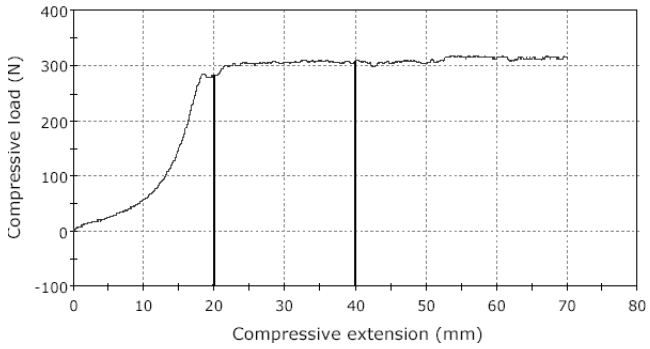

(i) A well behaved profile (Φ=3.93mm L/D=26.21 V_{beam}=0.4mm/s)

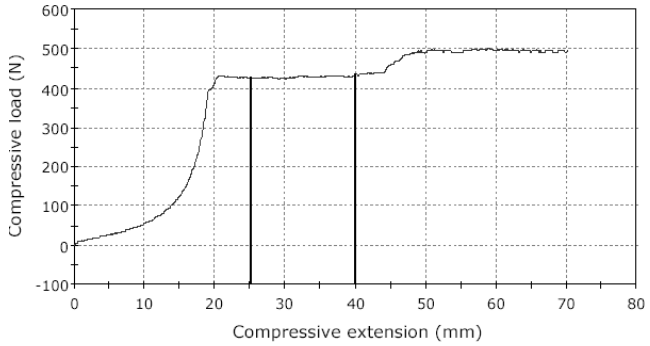

(ii) A profile with sudden jump (Φ=2.84mm L/D=30.4 V_{beam}=1mm/s)

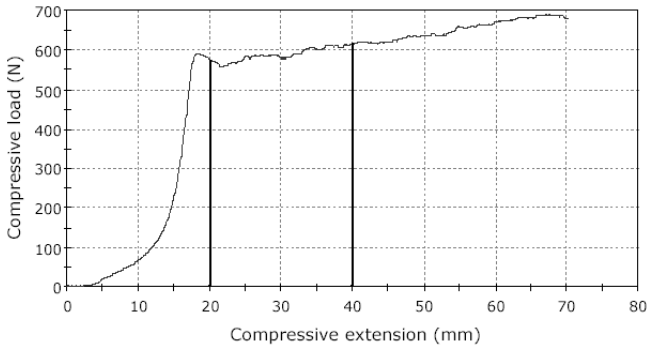

(iii) A profile with gradual increase (Φ=4.83mm L/D=30.4 V_{beam}=0.8mm/s

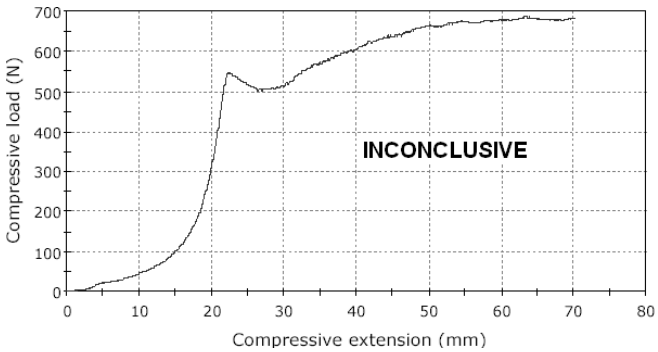

(iv) An inconclusive profile (Φ=3.93mm L/D=50.75 V_{beam}=0.6mm/s)

Figure 5.1 A range of extrusion force profiles with marked interpretations of steady state

5.2 Bagley plots

The data from both the unmarked extrusions and the corresponding marked ones were all plotted together, giving a maximum of eight points (dependant on conclusive force profiles and glass capillary damage that took place), from which to calculate a gradient by linear regression. It was decided that this form of averaging would be the most inclusive and accurate way to obtain a gradient from experiments that typically display a lot of scatter.

Figures 5.2 – 5.9 present an example set of raw data used. They show the individual force profiles and the ranges over which the extrusion force was averaged to produce the Bagley plot shown in Figure 5.10. The equation that appears in the top left corner of the graph represents the equation of the linear trend line through the points and has units of Pa. Hence for this particular diameter and flow rate, $4\tau_w$ is constant at 4730.9 Pa and τ_w at 1182.7 Pa.

Confidence has been taken in the assumption that the staining has not significantly affected the rheological behaviour of the potato from the relatively low levels of scatter observed when considering both sets of data simultaneously.

This process was repeated for the full range of flow rates and capillary diameters and allowing for damaged capillaries, involved 122 separate extrusions. Given that each extrusion took on average 30 minutes to set up and complete (not including paste preparation time), it is understandable why so many past attempts at Mooney analysis have used only three diameters and L/D ratios.

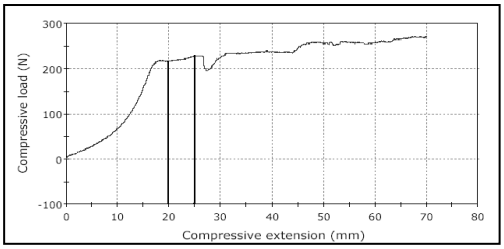

Figure 5.2 Set 1 Φ=3.93mm L/D=26.21 V_{beam}=0.2mm/s

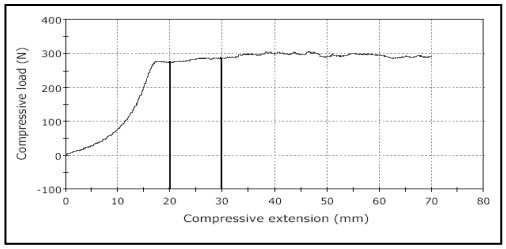

Figure 5.3 Set 1 Φ=3.93mm L/D=30.4 V_{beam}=0.2mm/s

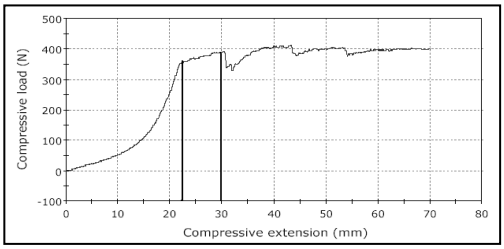

Figure 5.4 *Set 1 Φ=3.93mm L/D=39.4 V_{beam}=0.2mm/s*

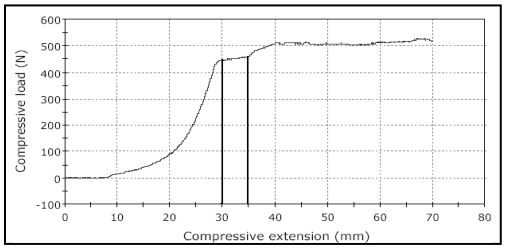

Figure 5.5 *Set 1 Φ=3.93mm L/D=50.75 V_{beam}=0.2mm/s*

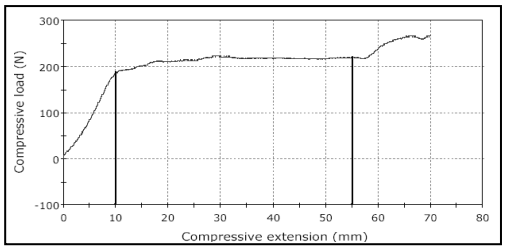

Figure 5.6 *Set 2 Φ=3.93mm L/D=26.21 V_{beam}=0.2mm/s*

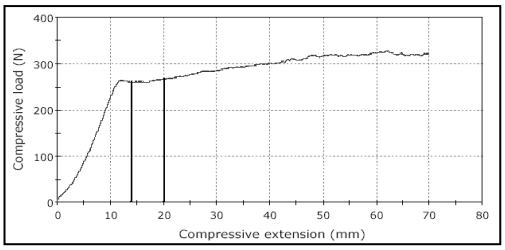

Figure 5.7 *Set 2 Φ=3.93mm L/D=30.4 V_{beam}=0.2mm/s*

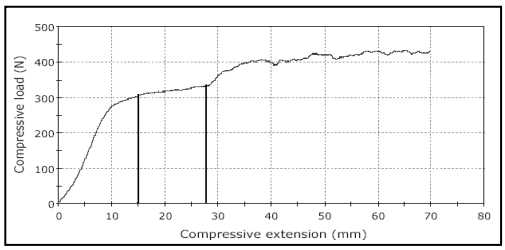

Figure 5.8 *Set 2 Φ=3.93mm L/D=39.4 V_{beam}=0.2mm/s*

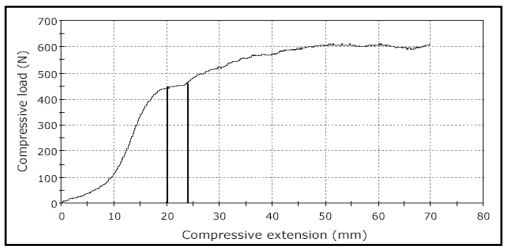

Figure 5.9 *Set 2 Φ=3.93mm L/D=50.75 V_{beam}=0.2mm/s*

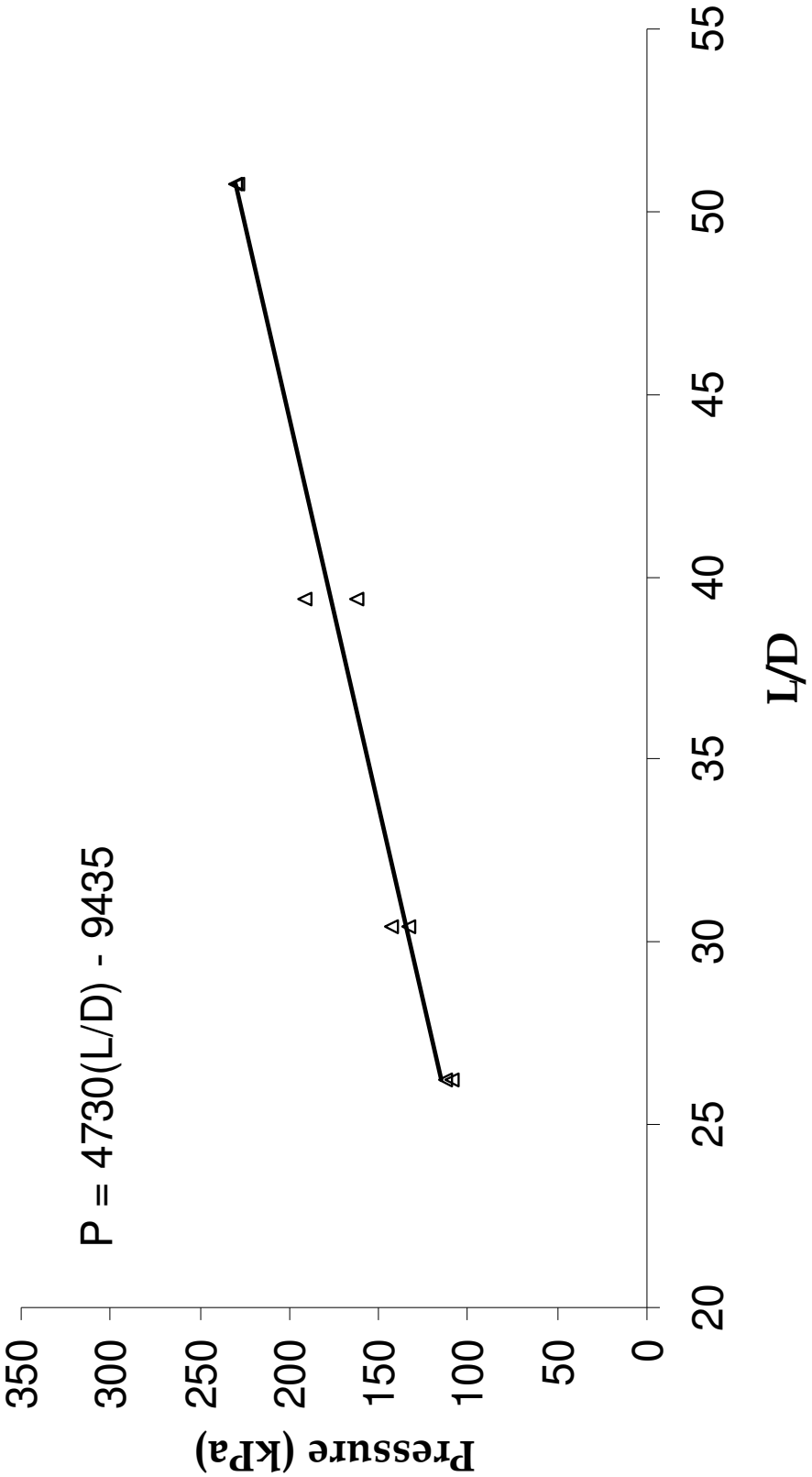

Figure 5.10 Bagley plot showing extrusion pressure against capillary L/D for Φ=3.93mm Q=9.82x10^{-8}m^3/s

5.3 Flow curves

With values of wall shear stress now obtained for a range of capillary diameters and flow rates, it is possible to construct a plot of wall shear stress, τ_w, against apparent shear rate, $\dot{\gamma}_A$, for each diameter (flow curve). The results of this plot are shown in Figure 5.11.

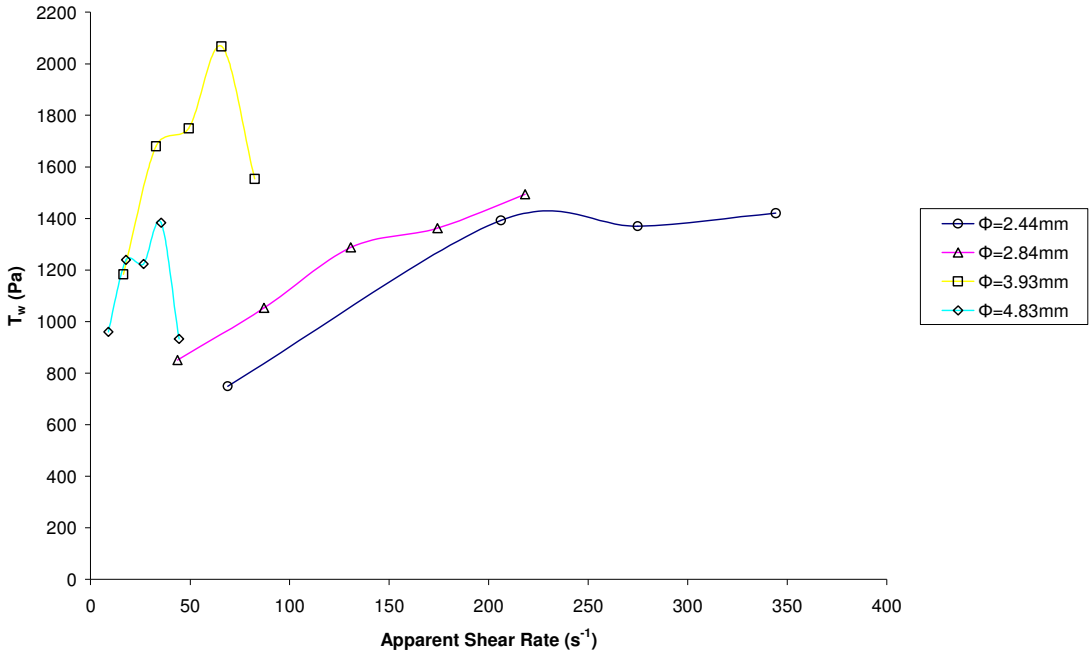

Figure 5.11 Flow curves obtained using all data points

Whilst the flow curves generally represent behaviour that would be expected (recall Figure 1.7), the falls in τ_w shown at the highest flow rates (the right most points), for the 3.93mm diameter and 4.83mm diameter, do not. Since these unexpected drops were first noticed after conducting the analysis on the unmarked data only, the water content of the colour marked extrudate was subsequently measured in order to monitor the composition of the paste after extrusion.

5.4 Extrudate water content

The results of the repetitions showed a similar trend (hence the maintained presence of the low points in Figure 5.11). However, the results of the extrudate water content analysis conducted on the colour marked experiments offered some possible explanation for their occurrence.

Table 5.1 shows the average percentage increase in water content of the extrudate for each extrusion flow rate and highlights the greatest change occurring during the 4.91×10^{-7} m^3/s extrusions.

Extrusion Flow Rate (m^3/s)	Average change in water content (%)
9.82×10^{-8}	+0.7
1.96×10^{-7}	+2.1
2.94×10^{-7}	-0.1
3.92×10^{-7}	-1.3
4.91×10^{-7}	**-4.9**

Table 5.1 Average water content change for each extrusion flow rate

Liquid phase migration involves changes in the solids volume fraction due to local movements of the liquid phase and hence a stiffening or lubrication of the paste. According to Wilson & Rough (2006), it is determined by the ratio of time taken for the paste to pass through the deformation zone at the die entry and the time taken for the liquid phase to move through the paste matrix in response to pore pressure (recall the addition of glycerol to the liquid phase in the Talc paste to limit liquid drainage).

It is generally considered that dilation occurring in the entry region of the die due to rearrangement of the matrix, leads to increased voidage and draws liquid from other regions. This can lead to the build up of drier static zones around the die entry, as verified visually by Bayfield et al. (1998). This behaviour, associated with low flow rates, leads to a wetter extrudate and has possibly occurred on a small scale with the two smallest flow rates above.

Studies by both Wilson & Rough and Bayfield showed that the effect of liquid phase migration was less apparent at higher flow rates, leaving the near 5% decrease in water content for the highest flow rate as unusual when considering the classic phase migration model. However, it is quite possible that the higher extrusion flow rates could have caused a micro structural change in the entry region with a reduced voidage as a result. Evidence was also found in the literature of a model developed by Rough et al. (2002) that predicted wetter extrudates at low flow rates but drier extrudates at intermediate flow rates. No experimental verification of this was found.

Whilst the extrudate for these extrusions is drier than the barrel paste and it may have been expected that any liquid phase migration would lead to increased water content, the material has none the less undergone an unexplained change in composition. Comfort can no longer be taken that the material for these particular experiments has remained reasonably homogenous and the anomalous data points can legitimately be omitted.

5.5 Presence of wall slip

The revised flow curves are shown in Figure 5.12 over the page. Indicative of a Herschel-Bulkley material (see Section 1.2), it seems appropriate to fit a power law trend line to each diameter. Based on the theory of the Mooney model, the final plot goes someway to indicate that wall slip is occurring in the potato paste. The rearranged Mooney Equation (5) is recalled as:

$$\frac{32Q}{\pi D^3} = \frac{8}{D} V_{slip} + \frac{4}{\tau_w^3} \int_{\tau_0}^{\tau_w} \left(\frac{\tau - \tau_0}{K} \right)^{\frac{1}{\lambda}} \tau^2 d\tau$$

Without the presence of wall slip, all of the plotted points would lie on a single curve, since for any constant value of τ_w, there would be a single apparent shear rate for all diameters and the Mooney plot of $\dot{\gamma}_A$ against 8/D would be horizontal with no gradient and hence no slip. Consequently, the upwards shift of the curves with increasing diameter indicates the presence of slip. The data however is not entirely conclusive on this matter as there is little or no shift of the 4.83mm diameter curve from the 3.93mm diameter curve, as would be expected. This, however, is beneficial to the project as it is desirable to be analysing a paste which does not conform perfectly to the Mooney model.

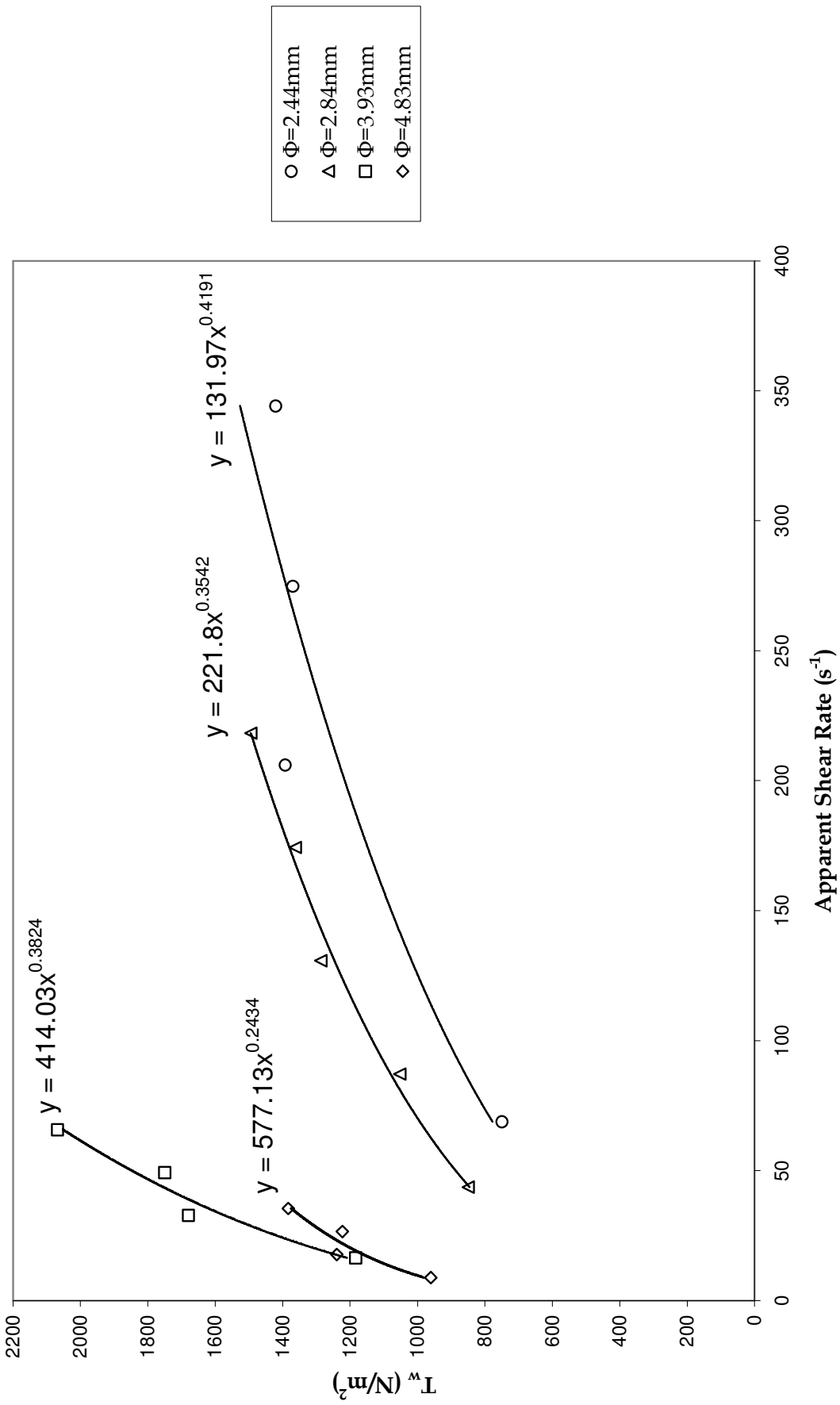

Figure 5.12 Revised flow curve

5.6 Graphical methods of predicting slip velocities

In order to conduct both Mooney analysis and Jastrzebski analysis graphically, lines of constant τ_w must pass clearly through multiple curves to generate multiple values of $\dot{\gamma}_A$, corresponding to each diameter of capillary.

The range of wall shear stress values chosen in this case is shown in Figure 5.13. This region of 1050 - 1400 Pa at 50 Pa intervals was chosen so as to generate at least three available points for all values of τ_w. Whilst it would have been desirable to generate four intersections for all values of τ_w by extrapolating the flow curves for the two larger diameters, this would have resulted in Mooney and Jastrzebski plots that were not constructed entirely with recorded data. As such, only four intersection points were used when the position of the flow curves allowed it.

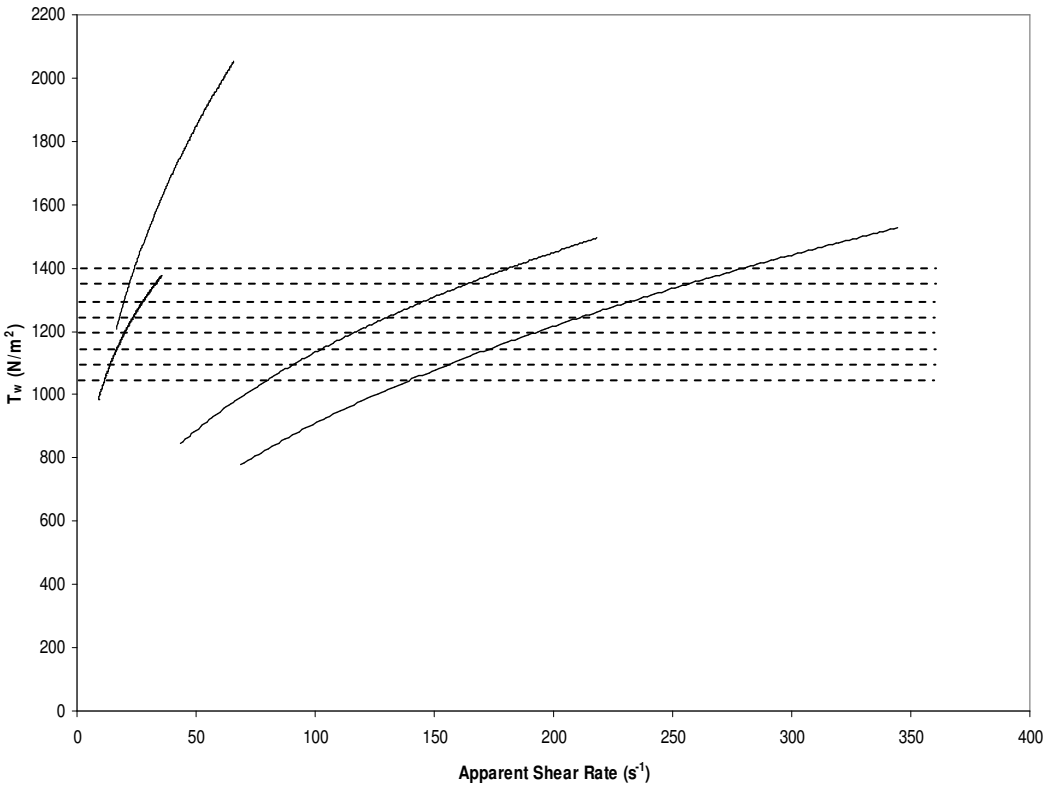

Figure 5.13 Constant values of τ_w chosen to give at least three points on all Mooney plots

5.7 Mooney plots

The intersection points shown in Figure 5.13 now provide the data to construct Mooney plots for eight values of τ_w, plotting $\dot{\gamma}_A$ against 8/D. An example of one of these Mooney plots is shown below in Figure 5.14.

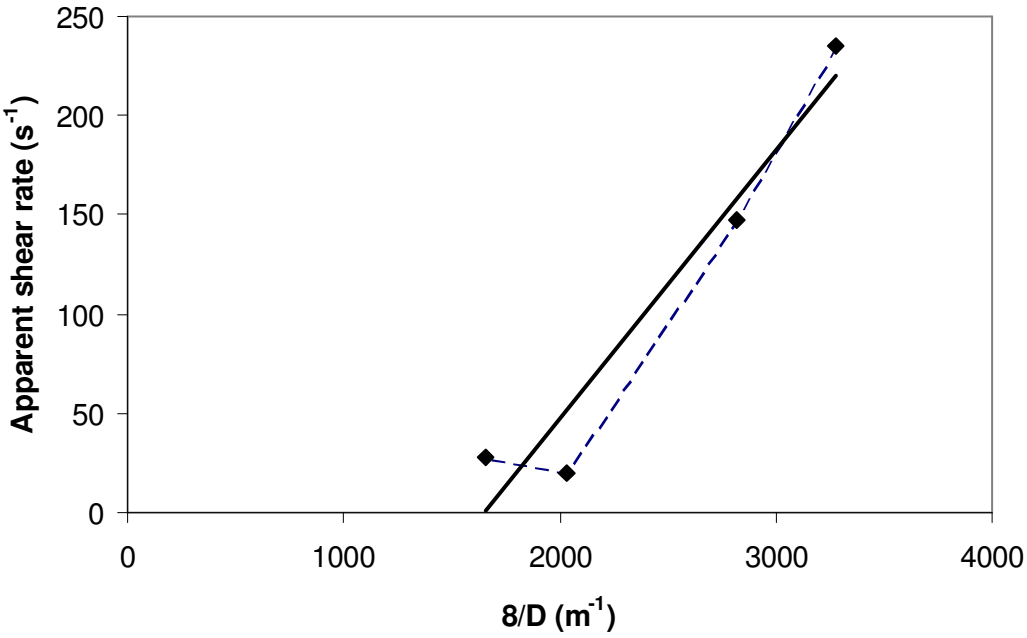

Figure 5.14 Mooney plot constructed for τ_w *= 1300Pa*

The graphs represent an unviable Mooney plot (indicative of all eight values of τ_w) under either of the following interpretations:

1. The plot is not clearly linear as stipulated by the Mooney model. Under these circumstances, the model does not apply and no slip velocity can be deduced.
2. If the plot is taken to be linear and a trend line applied, the intercept is negative. When considering the physical meaning of the Mooney equation, there are two contributions to the flow; the first term represents the contribution due to slip and the second term represents the contribution due to bulk shear. This contribution from bulk shear

is therefore the intercept of a Mooney plot, giving three possible scenarios: (i) the intercept is positive and there is positive flow due to bulk shear; (ii) the intercept passes through the origin and the flow comes from slip only; (iii) the intercept is negative indicating reverse bulk shear flow. The last of these three options is impossible as can be seen by imagining the velocity profile of all three cases shown in Figure 5.15.

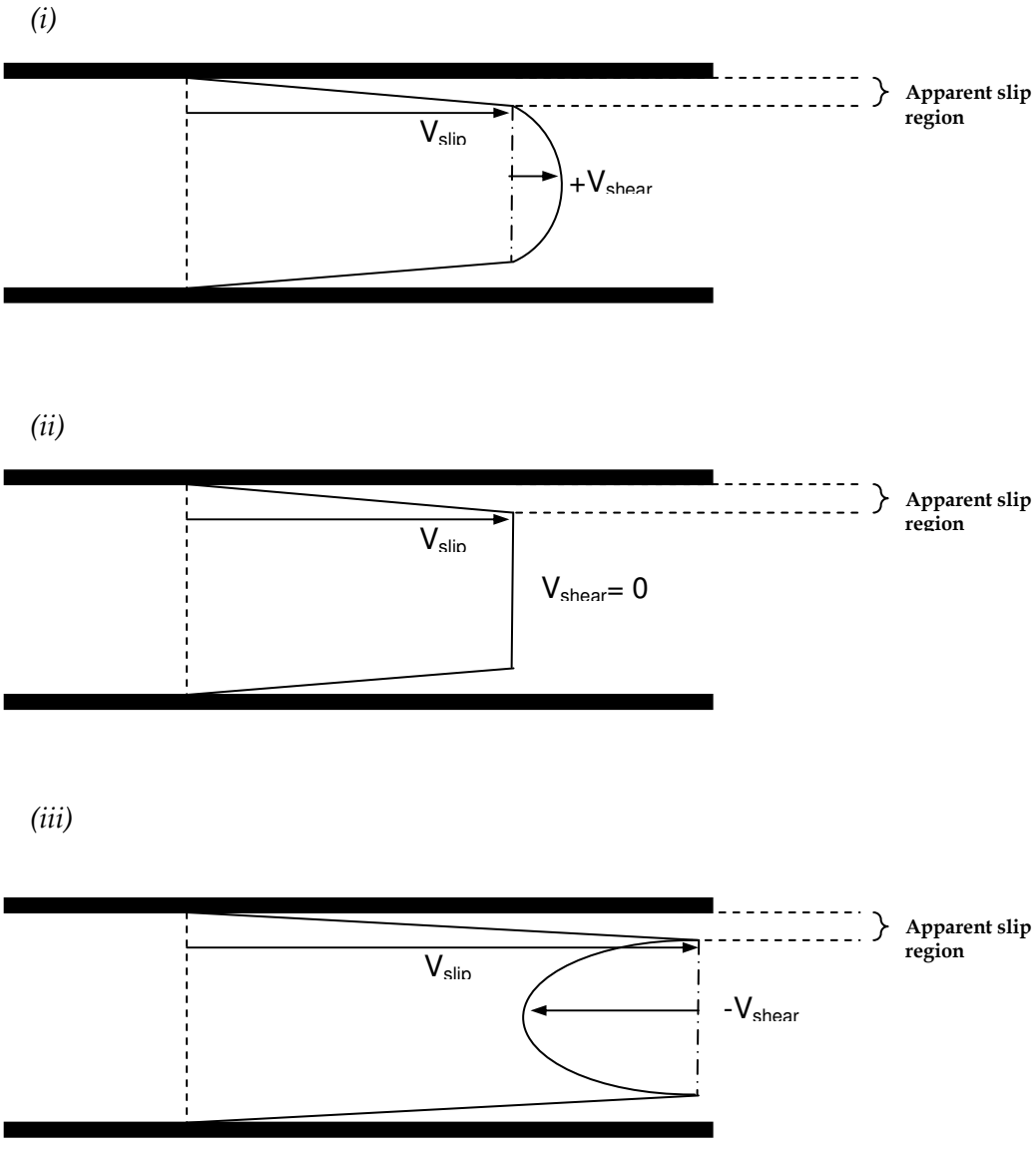

Figure 5.15 Velocity profiles indicative of (i) a positive Mooney plot intercept (ii) a Mooney plot intercept passing through the origin (iii) a negative Mooney intercept (impossible)

5.8 Considered use of Tikhnov regularisation

The graphical approach to conducting the Mooney analysis has been evaluated in the past by Corfield et al. (1999), citing the method as inefficient as it does not utilise all of the data, introduces a new source of error and does not allow for a systemic approach to dealing with any errors in experimental data.

An alternative numerical method based on Tikhnov regularisation was presented by Yeow et al. (2000, 2003) which addresses all three of the associated problems above and can be considered as an improved approach to applying Mooney's model. In Martin & Wilson's (2004) critical assessment of the Jastrzebski interface condition, three cases were cited of the successful application of Tikhnov regularisation to data where previous attempts at Mooney plots had been unsuccessful, including Jastrzebski's original data.

Access was available to programmable code which implemented this Tikhnov regularisation, but it was not considered an efficient use of time to apply the method when the data so strongly suggested unviable Mooney plots (particularly the positioning of the 4.83mm flow curve). Recalling the aims of the project, it was desirable that the paste being researched did not provide viable Mooney plots so as to require the use of the Jastrzebski method.

5.9 Jastrzebski interface condition

With the Mooney analysis unsuccessful, the potato granule and water paste would be an ideal candidate for use of the Jastrzebski interface condition. Recalling the work of Jastrzebski (1967), it was proposed that the slip velocity was a function of the wall shear stress and inversely dependant on the capillary diameter such that:

$$V_{slip} = \frac{f(\tau_w)}{D} \tag{9}$$

and hence:

$$\tau_w = \beta_j V_{slip} D \tag{10}$$

Substituting this into the rearranged Mooney equation (5) gives:

$$\frac{32Q}{\pi D^3} = \frac{8}{D^2}\frac{\tau_w}{\beta_j} + \frac{4}{\tau_w^3}\int_{\tau_0}^{\tau_w}\left(\frac{\tau-\tau_0}{K}\right)^{\frac{1}{\lambda}}\tau^2 d\tau \tag{11}$$

A plot of apparent shear rate against $8/D^2$, at constant τ_w, should be linear and the coefficient β_f may be calculated from the gradient. Figure 5.16 shows the Jastrzebski plot for the same value of τ_w used for the Mooney plot. Despite showing an improvement in both areas, the plots are still not confidently linear and still have a negative intercept, albeit closer to the origin. Unfortunately, it seems that the Jastrzebki method for predicting slip velocities has produced improved, but still unviable results.

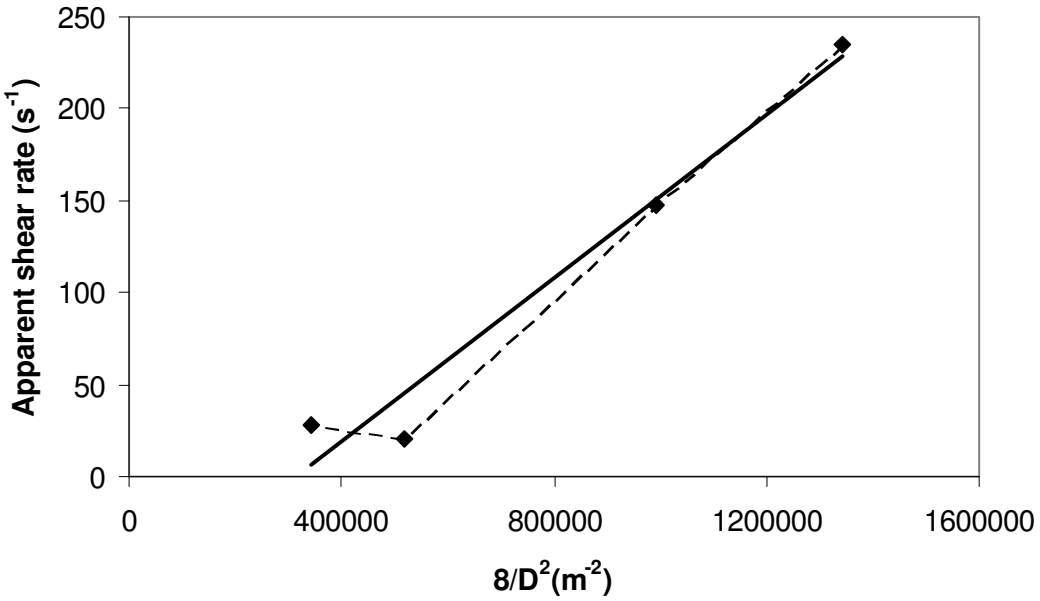

Figure 5.16 Jastrzebski plot constructed for τ_w = 1300Pa

5.10 Floating power method

Without any conclusive slip velocities predicted by the Mooney or Jastrzebski methods, there is no predicted data to compare with the slip velocities observed visually. As such, one final alternative analysis used by Cheng (1984) and titled here only as the 'floating power method' is to presume that Jastrzebski was correct to assume that the slip velocity was inversely dependant on the diameter, but that the power by which it was raised was not fixed at one, such that:

$$V_{slip} = \frac{f(\tau_w)}{D^m} \tag{12}$$

and hence:

$$\tau_w = \beta_f V_{slip} D^m \tag{13}$$

Substituting this instead into the Mooney in a similar fashion gives:

$$\frac{32Q}{\pi D^3} = \frac{8}{D^{m+1}} \frac{\tau_w}{\beta_f} + \frac{4}{\tau_w^3} \int_{\tau_0}^{\tau_w} \left(\frac{\tau - \tau_0}{K} \right)^{\frac{1}{\lambda}} \tau^2 d\tau \tag{14}$$

The power m is then altered manually until a linear plot of apparent shear rate against $8/D^{m+1}$ for constant τ_w with positive intercept is found. The coefficient β_f can then be calculated from the gradient. Figure 5.17 shows the successful floating power plot obtained from the potato granule data for the same value of τ_w and a manually chosen value of m = 3.8:

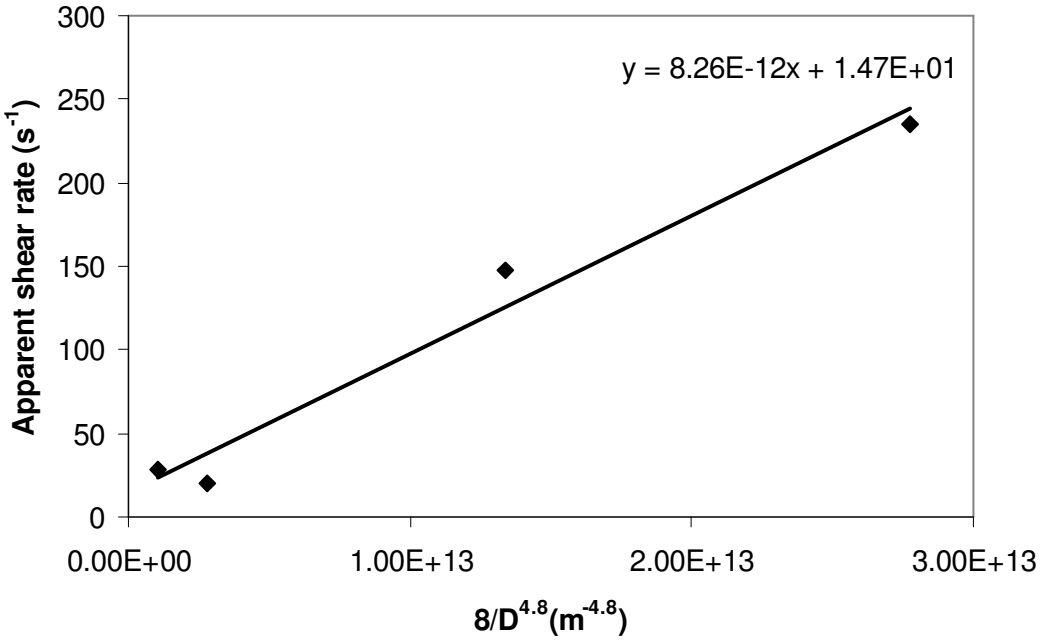

Figure 5.17 Floating power plot constructed for τ_w *= 1300Pa*

5.11 Obtaining predicted slip velocities

So as not to rule out the possibility that the Jastrzebski condition applies, but has been hidden by some degree of experimental error, it was decided to use both Jastrzebski and floating power predicted slip velocities for comparison with the visual data, but with the linear trend line of the Jastrzebski plots forced to pass through the origin.

Figure 5.18 shows the variation of β_j and β_f with τ_w as determined from the gradients of forced Jastrzebski plots and floating power plots for the eight values of τ_w between 1050 Pa and 1400 Pa. Power law trend lines seem to provide the best fit and have been fitted to each plot, generating an equation which can then be used to determine appropriate slip coefficients for back substitution into equations (10) and (13), producing a predicted slip velocity for each value of τ_w and D used in the visual experiments.

(i)

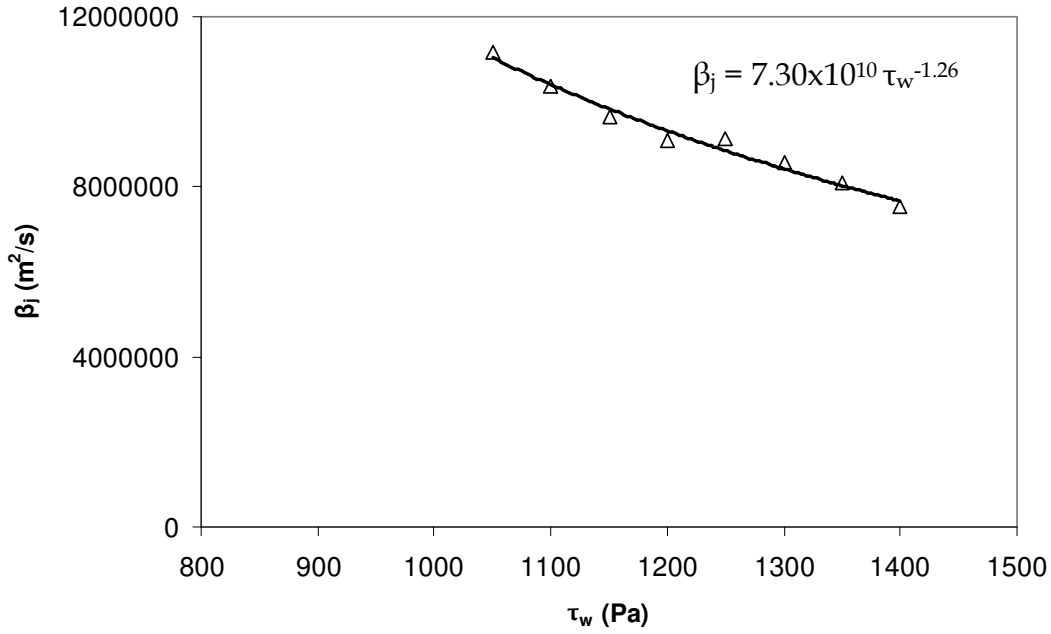

(ii)

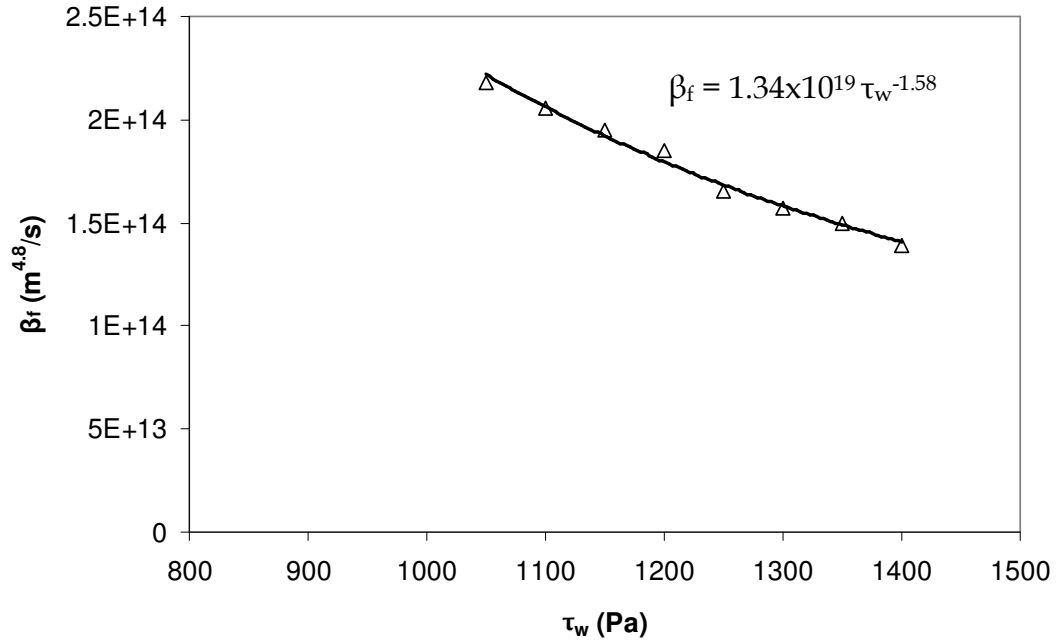

Figure 5.18 The variation of β_j and β_f with wall shear stress

5.12 Visually observed slip velocities

For each extrusion carried out in Set 2 (the colour marked experiments), the observed slip velocity was determined from the playback of the extrusion recording. An example of this is shown in Figure 5.19.

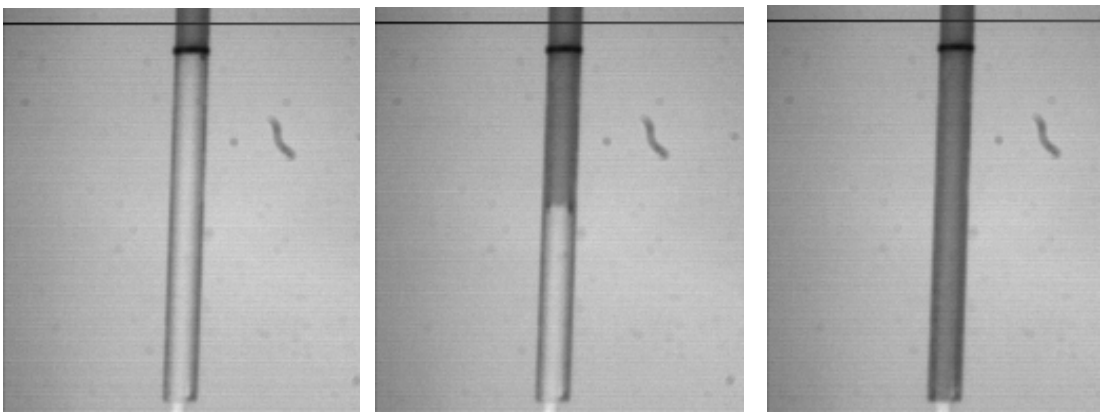

(i) *(ii)* *(iii)*

Figure 5.19 An example of a recording play back showing the position of the transition line for V_{beam} = 0.2mm/s Φ = 2.44mm L/D = 39.4 at (i) t =0.845s (ii) t = 2.756s (iii) t = 4.500s

The slip velocity was simply the distance, $L_{capillary}$, divided by the time taken for the transition line to pass through. With visual slip velocities successfully obtained for each extrusion, a comparison between predicted and observed slip velocities could now be made.

5.13 Comparison of predicted and observed slip velocities

Considering the earlier Bagley plots of Section 5.2 and the stipulation by both the Jastrzebki slip condition and the floating power slip condition that the slip velocity is a function of τ_w and D only, the extrusions at constant diameter and flow rate but varying L/D should all exhibit the same slip velocity. Consequently the recorded slip velocities for all L/D ratios at a fixed diameter and flow rate were averaged and used as the comparative visual slip velocities. The corresponding predicted slip velocities were then calculated by using the value of τ_w obtained from each Bagley plot to generate the coefficients β_j and β_f. These coefficients could then be used in equations (10) and (13) to generate predicted slip velocities from the two methods for that particular value of τ_w and D. The results of this comparison are shown below for each diameter:

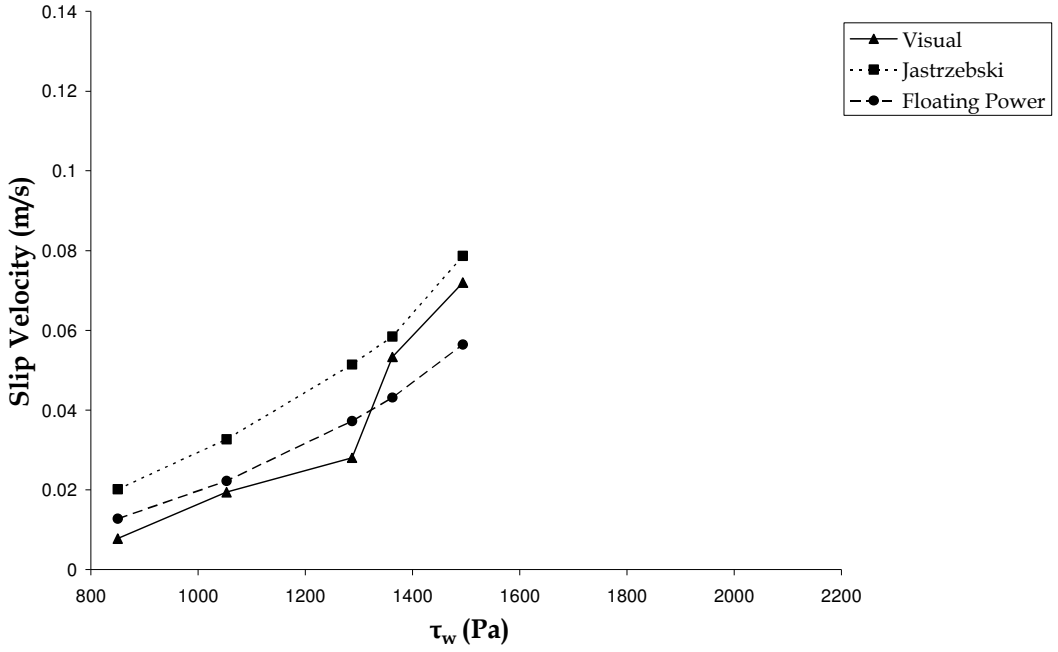

Figure 5.20 Comparison of predicted and observed slip velocities for 2.84mm diameter capillary

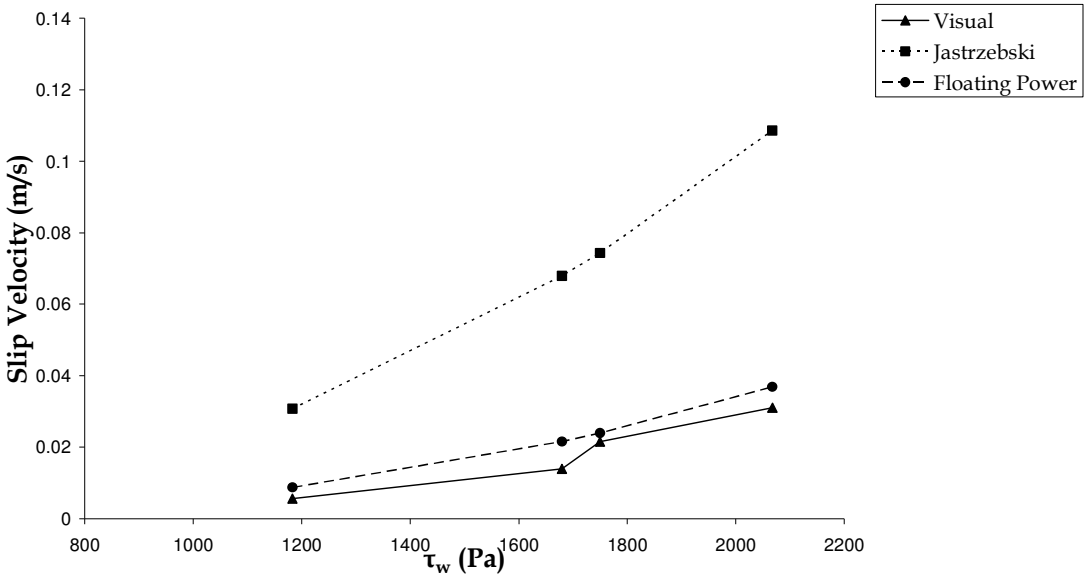

Figure 5.21 Comparison of predicted and observed slip velocities for 3.93mm diameter capillary

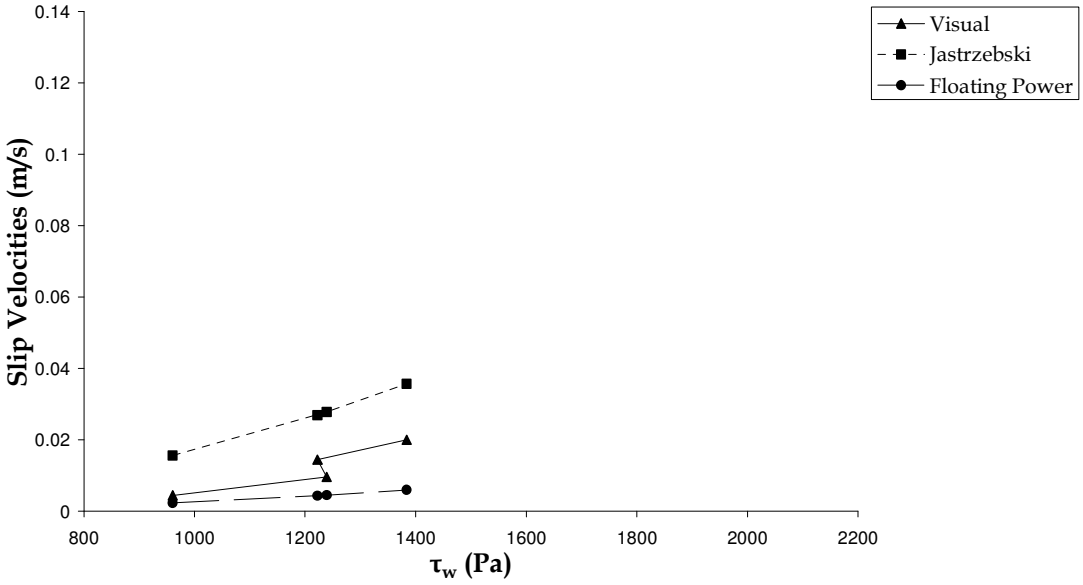

Figure 5.22 Comparison of predicted and observed slip velocities for 4.83mm diameter capillary

5.14 Interpretation

On first inspection, it can be seen that the two predictive methods both correctly predict the general trend of slip velocity behaviour, seemingly an increasing function of wall shear stress as hypothesised by Mooney.

However, it is the accuracy of these predictions which is of interest. For all three diameters, the Jastrzebski method significantly over-predicts the slip velocities for each value of τ_w. It is assumed that the visually observed slip velocities are correct, as there is no reason to suggest otherwise with accurate recordings and low levels of scatter. Given this, the average magnitudes of error in the Jastrzebski predictions at each value of τ_w for the diameters 2.84mm, 3.93mm, 4.83mm were 80%, 332% and 149% respectively. This cannot be considered a successful set of predictions under any circumstances and was wholly expected given the seemingly unviable Jastrzebski plots.

The floating power predictions seem to provide a better estimate without systematically over or under predicting. However, closer evaluation of the floating power errors suggests they only seem small in Figures 5.20, 5.21 and 5.22 due to the relative enormity of the Jastrzebski errors. The average magnitudes of error in the floating power predictions were 33%, 35% and 67% which again, cannot be regarded as acceptable estimates, especially since only one prediction from twelve was within 15% of the true slip velocity and none within 10%.

Further insight into the validity of the predictions can be gained by instead plotting the proportion of flow due to slip (Q_{slip}/Q) against τ_w as shown in Figures 5.23, 5.24 and 5.25. The redundancy of the Jastrzebski predictions is further highlighted by ratios of Q_{slip}/Q greater than unity (an impossible scenario) for all three diameters.

By similar reasoning, further doubt can be cast over the usefulness of the floating power method in this instance, with unviable flows due to slip predicted in the case of the 3.93mm diameter capillary (Figure 5.24).

It is concluded that in the particular range of extrusions and wall shear stresses studied for 67.1%wt. water with potato granules, the Jastrzebski and floating power methods for predicting slip velocities were wholly inaccurate.

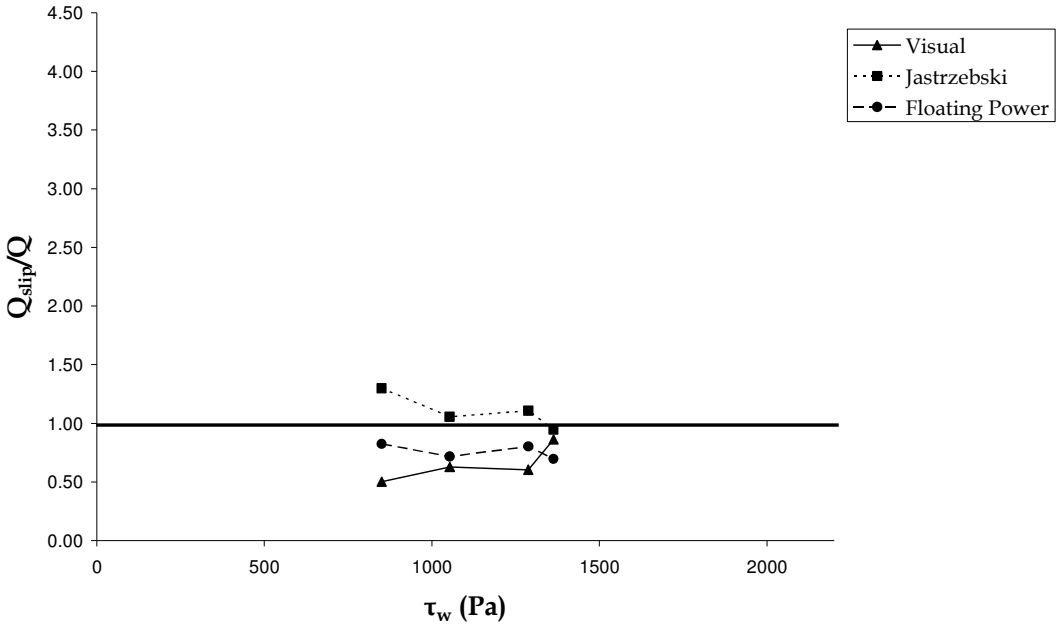

Figure 5.23 Predicted and observed Q_{slip}/Q for 2.84mm diameter capillary with the largest physical ratio permissible marked at 1

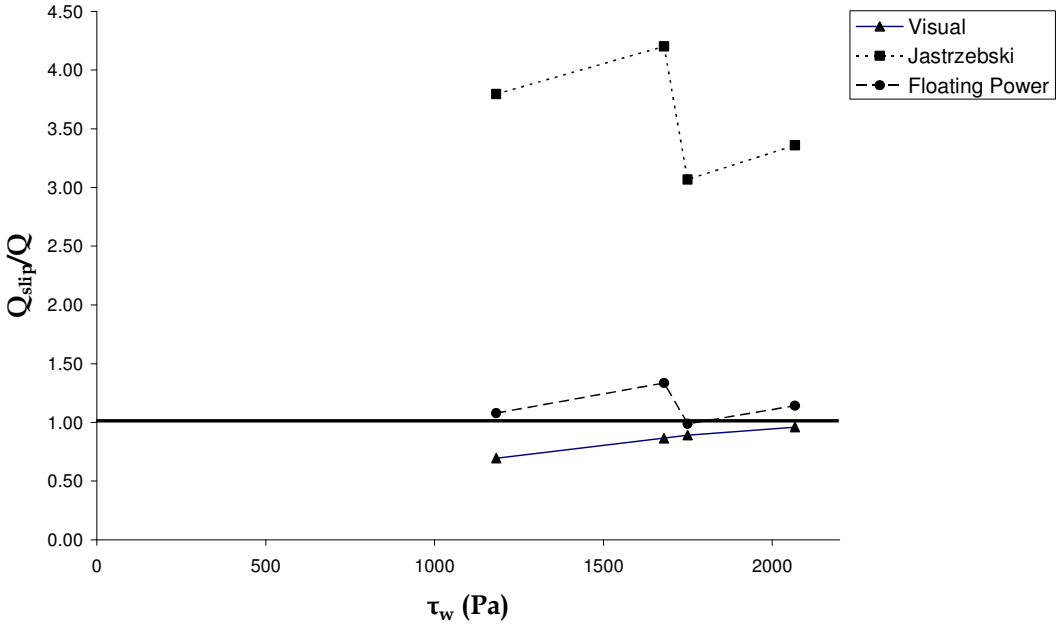

Figure 5.24 Predicted and observed Q_{slip}/Q for 3.93mm diameter capillary with the largest physical ratio permissible marked at 1

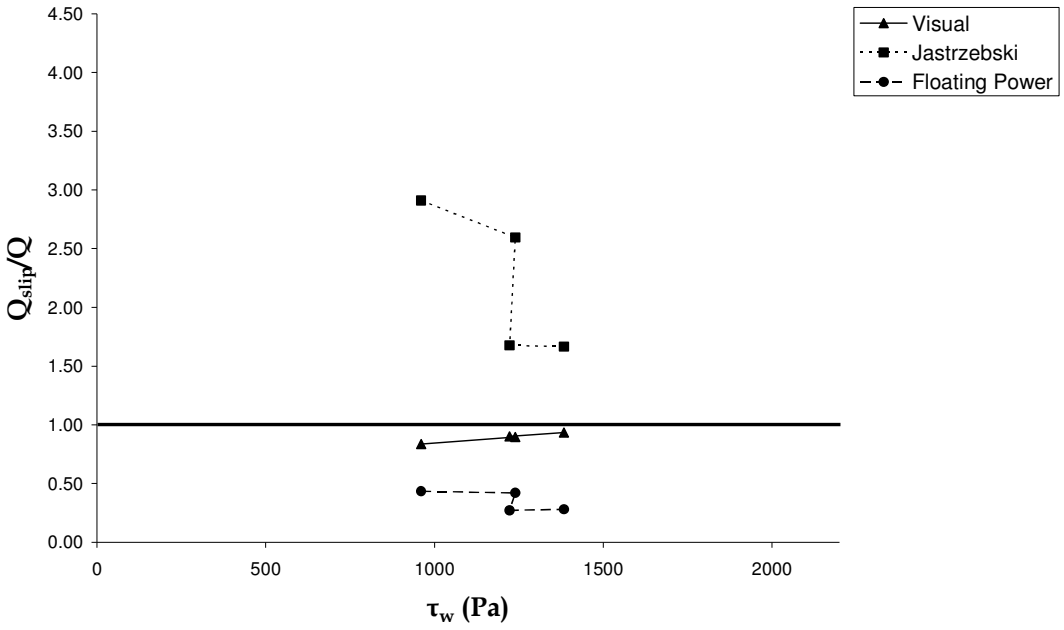

Figure 5.25 Predicted and observed Q_{slip}/Q for 4.83mm diameter capillary with the largest physical ratio permissible marked at 1

6 Conclusion

6.1 Restatement of aims

The purpose of this project was to provide some clarity on the validity of a particular method of analysis relating to the prediction of wall slip velocities in the extrusion of granular pastes.

Mooney (1931) proposed a theoretical model of paste flow in capillaries which said that a plot of apparent shear rate against 8/D for constant wall shear stress generated a linear plot with the gradient representing the slip velocity. In 1967, Jastrzebski reported paste flow results that did not provide linear Mooney plots, but were linear if plotted against $8/D^2$ instead. As such, he proposed that the slip velocity could be inversely proportional to the capillary diameter and his method has been adopted as a standard course of action where Mooney analysis has yielded unviable predictions.

It was proposed that the Jastzebski method of analysis may have only been a convenient fit to data for a particular range of experiments and that its use in modern wall slip analysis may provide wall slip velocities which, whilst viable, are incorrect. The project sought to develop an independent experimental procedure for measuring wall slip velocities in materials which provided unviable classic Mooney plots, so as to compare them with velocities predicted by the Jastrzebski method. It was hoped to provide some quantitative evidence so as to provide comfort on the validity of the Jastrzebski interface condition for the capillary flow of pastes.

6.2 Project overview

During the course of the study a material, namely potato granules and water, was found for which the classic Mooney analysis yielded unviable results. This was desirable as it is the scenario which most often results in the use of the Jastrzebski method. Using this material as the study paste, equipment and a repeatable experimental method were successfully designed around the principle of colour marking to visually record slip velocities through transparent capillaries. This equipment and methodology allowed for all of the extrusions necessary to conduct Mooney and Jastrzebski analyses, whilst simultaneously observing direct slip velocities from the same set of extrusions.

During the extrusions, the water content of the extrudate was monitored and for a particular range, significant liquid phase migration was observed.

As mentioned, the results of the Mooney analysis provided unviable results. Unfortunately, the slip velocities generated by the Jastrzebski method, whilst improved, were also unviable. So as to provide comparative data for the visually observed slip velocities, an alternative method of prediction known as the floating power method was used whilst also forcibly manipulating the Jastrzebki plots to provide viable results.

For the first time, it was possible to compare observed slip velocities with those predicted by the Jastrzebski method and the floating power method. This comparison showed that neither method predicted the slip velocities with a satisfactory level of accuracy. Due to time constraints, only the one material was successfully studied.

6.3 Discussion

Whilst this project has successfully been able to show the ineffectiveness of a Jastrzebski based method for one material over a particular range of wall shear stresses, it has gone no way to further explain why some pastes conform to the Mooney and Jastrzebski models whilst others do not. Many believe that the assumption of homogeneity in the bulk fluid is flawed in some pastes and that effects such as liquid phase migration undermine this basic assumption of the Mooney model. However, in this study, the extrudate composition was monitored and in the data used, only small degrees of phase migration were observed despite Mooney plots which were drastically unviable. The short comings of the Mooney model remain unknown.

The Jastrzebski interface condition suggests an influence of curvature and it is hard to critically assess the physical justifications of this when none were provided. Jastrzebski very loosely argued that the micro-structure of the bulk material could be affected by radius and so influence the amount of liquid phase available to form the slip layer, although this seems unlikely since most particle sizes are orders of magnitude smaller than the die radius (Wilson & Rough, 2006). It is also noted by Martin & Wilson (2005) that if the micro-structure is affected by capillary radius then its rheological properties are likely to change also, meaning that the Mooney analysis or any variation of it is invalid.

Unfortunately, the project has not been as conclusive as originally hoped, since although a material was found for which the Mooney method provided unviable results, the Jastrzebski results were also unviable and had to be manipulated to generate predicted slip velocities. Consequently, it is not possible to claim from this project that all viable slip velocities obtained using the Jastrzebski method are redundant. It can however be said that the Jastrzebski method should not be considered as a guaranteed fall back

approach to the Mooney method and further supports the claim that it should be used with caution.

However, when looking at the approaches used in this study from a retracted view point, the approach undertaken in applying the floating power method is no different in principle to that used by Jastrzebski - manipulating the dimensions of the Mooney plots until linear plots are achieved. In this instance, it has successfully been shown that the method has generated results, which, whilst mostly viable, are inaccurate.

6.4 Future work

The project undertaken has successfully generated a methodology to quantitatively assess slip velocities generated by predictive methods. However, time has not allowed sufficient experimentation to provide conclusive evidence to support or refute the effectiveness of the Jastrzebki interface condition as originally intended.

In order for this to be achieved, the comparative methods discussed in this project would need to be applied over a suitable range of materials for which the Jastrzebski method yielded viable results. This is recognised as a time consuming project, in which importance should be placed on completing extensive sets of data if complete comfort is to be achieved. The time intensive nature of Mooney and Jastrzebski analyses has, in the past, forced studies to perform extrusions with fewer capillary diameters than is acceptable when considering the large degrees of interpolation required. It is hoped that any further work undertaken in this area will be able to dedicate sufficient time so as to create flow curves with many data points for more than four diameters to give Mooney and Jastrzebski plots which can be interpreted reliably.

References

Adams MJ, Briscoe BJ, Sinha SK (1995) 'Interfacial and bulk rheological characterisations of paste materials in extrusion flow', 27th International SAMPE Technical Conference, 9-12 October 1995

Bayfield M, Hagget JA, Williamson J, Wilson DI, Zargar A (1998) 'Liquid phase migration in the extrusion of icing sugar pastes' Chemical Engineering Researc Design 76, 39-46

Corfield GM, Adams MJ, Briscoe BJ, Fryer PJ, Lawrence CJ (1999) 'A critical examination of capillary rheometry for foods (exhibiting wall slip)', Food and Bioproducts Processing, 77 (C1), 3-10

Cheng DCH (1984) 'Further observations on the rheological behavious of dense suspensions', Powder Technology, 37, 255-273

Coussot P, Ancey C (1999) 'Rheological classification of concentrated suspensions and granular pastes', Physical Review E, Volume 59, Number 4

Graczyk J, Buggisch H, Güner S (2001) 'Wall slip behaviour of alumina-silicone oil pastes during extrusion', Chemical Engineering Technology, Volume 24 (5) 489-491

Halliday PJ, Smith AC (1995) 'Estimation of the wall slip velocity in the capillary-flow of potato granule pastes' Journal of Rheology, 39 (1), 139-149

Halliday PJ, Smith AC (1997) 'Compaction and flow of potato starch and potato granules' Food Science and Technology International, 3 (5), 333-342

Herschel WH, Bulkley R (1926) 'Measurement of consistency as applied to rubber-benzene solutions', Proc. Am. Soc. Testing Materials Volume 26(2), 621-633

Jastrzebski ZD (1967) 'Entrance effects and wall effects in an extrusion rheometer during the flow of concentrated suspensions', Industrial and Engineering Chemistry Fundamentals, Volume 6 (3), 445-454

Khan Au, Briscoe BJ, Luckham PF (2001) 'Evaluation of slip in capillary extrusion of ceramic pastes', Journal of the European Ceramic Society, Volume 21 (4), 483-491

Kokini, JL, Plutchok GJ (1987) 'Viscoelastic properties of semisolid foods and their biopolymeric component', Food Technology, 41 (3), 89-85

Martin PJ (2002) 'Mechanics of paste flow in radial screen extruders', Dissertation, Department of Chemical Engineering, University of Cambridge

Martin PJ, Wilson DI, Bonnett PE (2004) 'Rheological study of a talc based paste for extrusion-granulation', Journal of the European Ceramic Society, Volume 24, 3155-3168

Martin PJ, Wilson DI (2005) 'A critical assessment of the Jastrzebski interface condition for the capillary flow of pastes, foams and polymers', Chemical Engineering Science, Volume 60, 493-502

Mooney M (1931) 'Explicit formulas for slip and fluidity', Journal of Rheology, 2, 210-222

Rough SL, Wilson DI, Bridgewater J (2002) 'A model describing liquid phase migration within an extruding microcrystalline cellulose paste', Chemical Engineering Research Design, 80, 701-714.

Segur JB, Oberstar HE (1951) 'Viscosity of glycerol and its Aqueous Solutions', Journal of Industrial and Engineering Chemistry, 43,2117

Shukla A, Rizvi SSH (1995) 'Measurement of the flowability of butter by capillary rheometry', Journal of Texture Studies, 26 (3), 299-311

Steffe, JF (1996) 'Rheological Methods in Food Process Engineering', Freeman Press, East Lansing, MI, USA

Wilson DI, Rough SL (2006) 'Exploiting the curious characteristics of dense solid-liquid pastes', Chemical Engineering Science, Volume 61, 4147-4154

Yeow YL, Nguyen YT, Vu TD, Wong HK (2000) 'Processing the capillary viscometry data of fluids with yield stresses', Rheologica Acta, Volume 39, 392-398

Yeow YL, Lee HL, Melvani AR, Mifsud GC (2003) 'A new method of processing capillary viscometry data in the presence of wall slip', Journal of Rheology, Volume 47 (2), 337-348

Appendices

Appendix 1 – Mooney equation derivation

For clarity, the derivation of the Mooney method shown below is based upon work from Martin (2002) which presents the work of Mooney in a clearer and more direct way than Mooney's original paper.

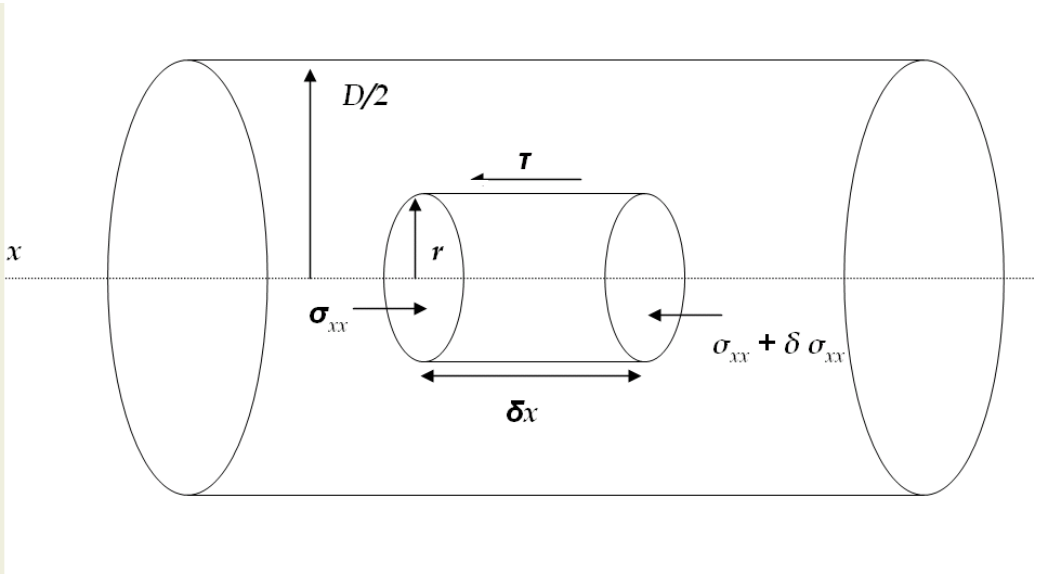

Figure A.1 Force balance over a central element of material

A force balance over a central element of material flowing in steady state as shown in Figure 1.6 yields:

$$-\frac{d\sigma_{xx}}{dx}=\frac{2\tau}{r}=\frac{4\tau_w}{D} \tag{15}$$

where, σ_{xx}, is the normal stress in the axial direction acting on the ends of the element, τ, is the shear stress acting in the axial direction, τ_w, is the shear stress acting in the axial direction at the wall, r is the element radius and D is the capillary diameter.

Integrating the flow through an annulus over the capillary cross-section gives the volumetric flow rate, Q:

$$Q=2\pi\int_0^{D/2}Vrdr \tag{16}$$

which can be separated into the slip and shear components of velocity:

$$Q=\frac{\pi D^2}{4}V_{slip}+2\pi\int_0^{D/2}V_{shear}rdr \tag{17}$$

Assuming that V_{shear} is a function of radial position (see Figure 1.5) and integrating by parts, gives:

$$Q=\frac{\pi D^2}{4}V_{slip}+\left[\frac{2\pi V_{shear}r^2}{2}\right]_0^{D/2}-\pi\int_0^{D/2}\frac{dV_{shear}}{dr}r^2dr \tag{18}$$

Realising that V_{shear} is equal to zero at the capillary wall (r = D/2), the second term disappears to leave:

$$Q=\frac{\pi D^2}{4}V_{slip}-\pi\int_0^{D/2}\frac{dV_{shear}}{dr}r^2dr \tag{19}$$

Rearranging the Herschel-Bulkley constitutive equation given earlier (2) gives:

$$\dot{\gamma} = \frac{dV_{shear}}{dr} = \left(\frac{\tau - \tau_0}{K} \right)^{\frac{1}{\lambda}} \tag{20}$$

and rearranging the force balance equation gives:

$$r = \frac{\tau D}{2\tau_w} \qquad \text{and} \qquad dr = \frac{D}{2\tau_w} d\tau \tag{21)(22}$$

Equations (20),(21) and (22) can then be substituted back into equation (19) to give:

$$Q = \frac{\pi D^2}{4} V_{slip} + \frac{\pi D^3}{8\tau_w^3} \int_{\tau_0}^{\tau_w} \left(\frac{\tau - \tau_0}{K} \right)^{\frac{1}{\lambda}} \tau^2 d\tau \tag{23}$$

Appendix 2 - COSHH Assessment form

The COSH assessment form required for the Magnesium Silicate is copied below.

COSHH Assessment Form

If insufficient space is available under any section, use a separate piece of paper and attach it to the form.	**Serial No:** **Date**:
Department: Engineering Science **Location of work: 3rd Floor Thom**	**Persons involved: Alasdair Walker, Peter Martin (Supervisor)**

Description of procedure: Talc powder is to be made into paste form by mixing with water in an industrial mixer before being transferred to a barrel and extruded through a capillary.

Substances used:	Quantities Used	Frequency of use	Hazards identified	Exposure route
Talc	*2kg*	*2 days a week*	*dust*	*inhalation*

Could a less hazardous substance (or form of substance) be used instead? **no**
Justify not using it:

What measures have you taken to control risk?

Engineering controls:

PPE:
Eye protection, lab coat, gloves, dust mask

Management measures:
Stored in sealed container

Checks on control measures:

Is health surveillance required? *no*	**Training requirements** *none*
Emergency procedures: **Fire:** *N/A* **Spillage***: Normal clean up procedure. Vacuum cleaning recommended to avoid airborne dust. No flush to sewer.*	**Waste disposal:** *Double bagged for normal bin disposal*
Name and position of assessor: Alasdair Walker (4YP Student)	**Signature:**
Name of supervisor (student work only): Peter Martin	**Signature:**
Name of head of department or nominee (DSO): Derek Reed	**Signature:**

Appendix 3 - Risk assessment

A copy of the two page risk assessment completed prior to this project is provided below.

Department of Eng Science

4th Year Project Risk Assessment

Form RA01 15/10/03

Risk Assessment	Wall Slip in Pasty Flows			Page 1 of 2
In Building	Thom			
Assessment undertaken	Alasdair Walker	Signed	Date :	
Assessment supervisor	Peter Martin	Signed	Date :	

Hazard	Persons at Risk	Risk Controls In Place	Further Action Necessary To Control Risk
General risk of bodily entrapment from large forces transmitted by Instron testing machine	Researcher/others in vicinity	Locking pins limit vertical range of movement. Screens in place during experiment runs. Maximum load trip.	Training package to be devised by Bob Scott/Igor Dyson and undertaken by researcher covering general use and safety features of machine
Muscular skeletal injury carrying heavy testing rig to Instron machine	Researcher	Transportation trolley for use between 3rd floor chemical lab and testing machine.	Rig to be carried using appropriate lifting technique. All rig components to be transported separately and constructed at testing machine.
Body/eye injury caused by projectile parts from test rig during compression	Researcher/others in vicinity	One flat safety screen at rear of testing machine Eye protection to be worn.	Second safety screen for front to be designed around video testing equipment
Congestion and cables across open floor space from potential lighting equipment	Researcher/others in vicinity	None	Ensure all equipment is arranged tidily and all loose cables are taped down

UPS 52/97

t

Department of Eng Science

4th Year Project Risk Assessment

Form RA01 16/10/03

Talc powder inhalation	Researcher/others in vicinity	See COSHH Assessment	See COSHH Assessment
Moving parts of industrial mixer	Researcher/others in vicinity	Safety guard in place.	None
240V Appliances	Researcher/others in vicinity	Equipment PAT tested by Electronics	Supervisor to check validity of PAT test label

Your E-mail Address: alasdair.walker@stcatz.ox.ac.uk..... Checked by ..... date .....

(D J Reed)

UPS S2/97

Appendix 4 – Cross beam velocity to flow rate conversions

The conversions between V_{beam} and Q were conducted using equation (24) and are shown in Table A.1.

$$Q = V_{beam} \times A_{barrel} \tag{24}$$

V_{beam} (mm/s)	Q (m^3/s)
0.2	9.82×10^{-8}
0.4	1.96×10^{-7}
0.6	2.94×10^{-7}
0.8	3.92×10^{-7}
1.0	4.91×10^{-7}

Table A.1 Conversions between values of V_{beam} used and the resulting Q